

***AKARI* Observations of Brown Dwarfs I.: CO and CO₂ Bands in the Near-Infrared Spectra**

Issei Yamamura

*Institute of Space and Astronautical Science (ISAS), JAXA, Yoshino-dai 3-1-1, Chuo-ku, Sagamihara,
Kanagawa 252-5210, Japan*

yamamura@ir.isas.jaxa.jp

and

Takashi Tsuji and Toshihiko Tanabé

*Institute of Astronomy, School of Science, The University of Tokyo, 2-21-1, Osawa, Mitaka, Tokyo,
181-0015, Japan*

ttsuji@ioa.s.u-tokyo.ac.jp, ttanabe@ioa.s.u-tokyo.ac.jp

ABSTRACT

Near-infrared medium-resolution spectra of seven bright brown dwarfs are presented. The spectra were obtained with the Infrared Camera (IRC) on board the infrared astronomical satellite *AKARI*, covering 2.5–5.0 μm with a spectral resolution of approximately 120. The spectral types of the objects range from L5 to T8, and enable us to study the spectral evolution of brown dwarfs. The observed spectra are in general consistent with the predictions from the previous observations and photospheric models; spectra of L-type dwarfs are characterized by continuum opacity from dust clouds in the photosphere, while very strong molecular absorption bands dominate the spectra in the T-type dwarfs. We find that the CO fundamental band around 4.6 μm is clearly seen even in the T8 dwarf 2MASS J041519–0935, confirming the presence of non-equilibrium chemical state in the atmosphere. We also identify the CO₂ fundamental stretching-mode band at 4.2 μm for the first time in the spectra of late-L and T-type brown dwarfs.

As a preliminary step towards interpretation of the data obtained by *AKARI*, we analyze the observed spectra by comparing with the predicted ones based on the Unified Cloudy Model (UCM). Although overall spectral energy distributions (SEDs) can be reasonably fitted with the UCM, observed CO and CO₂ bands in late-L and T-dwarfs are unexpectedly stronger than the model predictions assuming local thermodynamical equilibrium (LTE). We examine the vertical mixing model and find that this model explains the CO band at least partly in the T-dwarfs 2MASS J041519–0935 and 2MASS J055919–1404. The CO fundamental band also shows excess absorption against the predicted one in the L9 dwarf SDSS J083008+4828. Since CO is already highly abundant in the upper photospheres of late-L dwarfs, the extra CO by vertical mixing has little effect on the CO band strengths, and the vertical mixing model cannot be applied to this L-dwarf. A more serious problem is that the significant enhancement of the CO₂ 4.2 μm band in both the late-L and T dwarfs cannot be explained at all by the vertical mixing model. The enhancement of the CO₂ band remains puzzling.

Subject headings: molecular processes — stars: atmospheres — stars: late-type — stars: low-mass, brown dwarfs —

1. Introduction

Brown dwarfs are defined as the objects that were born as isolated objects but were not massive enough to ignite hydrogen nuclear burning (Burrows et al. 2001). They are particularly of interest for their extremely low-temperature atmospheres in relation to giant planets. Observational studies of brown dwarfs have been extensively carried out since the first definitive identification of a genuine brown dwarf Gl 229B (of the class now known as T-dwarf) by Nakajima et al. (1995). The first L-type brown dwarf GD 165B was reported by Becklin & Zuckerman (1988) although it was debated for some time whether it was a star or a brown dwarf. This very red object is important in that the presence of dust layer in the photosphere was recognized for the first time by this object (Tsuji et al. 1996). Spectroscopic observations in the infrared regime are the most essential tools to obtain physical and chemical information of brown dwarfs, through absorption bands of various molecules in the atmospheres.

Carbon monoxide (CO) plays a decisive role in determining the major characteristics of cool stars because of its very large dissociation energy (Russell 1934). In brown dwarfs, the CO first overtone band at $2.3\ \mu\text{m}$ is observed until early-T type sources (see e.g., Geballe et al. (2002) and Burgasser et al. (2006b)). The role of CO, however, changes in very cool dwarfs: carbon resides mostly in CH_4 rather than in CO in a very cool (e.g. $T \approx 1000\text{K}$) and high density (e.g. $\log P_g \approx 6.0$) environment (Tsuji 1964), and CO no longer plays any critical role under such a circumstance. Although no celestial object outside our Solar system having such a physical condition had been known, it was found at last that such a case is actually realized in the brown dwarf Gl 229B showing strong CH_4 bands (Oppenheimer et al. 1995).

However, nature is not so simple as predicted by a simple theory of thermochemistry. In fact, it was not long before an unexpected detection of CO fundamental band at $4.6\ \mu\text{m}$ in Gl 229B, classified as T6, was reported by Noll, Geballe, & Marley (1997) and Oppenheimer et al. (1998). These pioneering observations highlighted roles of non-equilibrium chemical processes. The idea of vertical mixing was suggested by Griffith & Yelle (1999) and Saumon et al. (2000). Because of the

extreme stability of CO, the chemical time scale is much longer than the mixing timescale and CO is dredged up by vertical mixing from the inner part of the atmosphere where CO is still abundant to the surface layers where CH_4 dominates instead of CO. Recently two more late-T dwarfs were found to show the CO band by Geballe et al. (2009), confirming that the presence of CO is a general characteristic of late-T dwarfs.

It is to be remembered that the observations so far are limited to late-T dwarfs. Observations of the CO fundamental band in early-T and L-type dwarfs are needed for a unified understanding of the physical and chemical processes related to CO in the atmospheres of brown dwarfs. Spectroscopic observations of the CH_4 and of the CO transitions in *L* and *M*-band are always difficult from the ground. Severe atmospheric absorption and limited wavelength coverage make precise analysis difficult. Thus, there is a strong motivation to carry out near-infrared spectroscopy of brown dwarfs from space, especially in the region of $2.5\text{--}5.0\ \mu\text{m}$ which remains the least explored so far.

The infrared astronomical satellite *AKARI* (Murakami et al. 2007) was launched in 2006 February. Scientific observations under cryogenic condition were carried out from 2006 May to 2007 August, and ended with the liquid Helium boil-off. The satellite is equipped with a 68.5 cm cooled telescope and two scientific instruments covering the wavelength range of $1.8\text{--}180\ \mu\text{m}$. One of them, the Infrared Camera (IRC; Onaka et al. 2007) carried out imaging and spectroscopic observations in the near- to mid-infrared wavelength regions. The IRC provided a unique opportunity to take spectra of brown dwarfs in the range between 2.5 and $5.0\ \mu\text{m}$ without interference of telluric absorption from the atmosphere. In the framework of the *AKARI* Mission Programme (MP; coordinated observations by the project team members), we have carried out a series of near-infrared spectroscopic observations of ultracool dwarfs. This programme, *NIRLT* (PI: I.Yamamura), aims to obtain a set of legacy data for studies of the evolution of physical and chemical structure of L- and T-dwarfs. In this paper we present the initial results from this programme.

As a basis of interpretation of the spectra observed with *AKARI*, we determine basic physical parameters of six well observed objects. For

this purpose, we apply model photospheres as in the analyses of ordinary stars. However, the model photospheres of ultracool dwarfs including brown dwarfs are by no means well established yet. It has been discussed that dust grains in the atmosphere play an important role in the formation of spectra of ultracool dwarfs: especially spectra of L-type dwarfs ($T_{\text{eff}} = 2200\text{--}1400\text{ K}$) are strongly influenced by the continuous opacity of dust, while spectra of even cooler T-type dwarfs are dominated by deep molecular absorption bands (Tsuji et al. 1996). In particular, we have no definite guideline for treating dust formation in the photosphere. Some attempts to model the photospheres of brown dwarfs with dust clouds have been carried out by several groups and these are discussed in detail by Helling et al. (2008). It was shown that all models agree on the global structure of the dusty photospheres, but predicted features such as the emergent spectra differ considerably, depending on the opacity data and reflecting the extreme complexity of such objects.

We apply the Unified Cloudy Model (UCM: Tsuji 2002, 2005) as an example of such dusty model photospheres to the analysis of our objects. We assume Solar metallicity throughout, and estimate T_{eff} , T_{cr} (critical temperature that defines the upper boundary of the dust cloud; see Section 4.1 for detail), and $\log g$ from the relative SEDs (i.e. shapes of the spectra). We then fit the observed and predicted spectra on an absolute scale and estimate the radii of individual objects with the use of the known parallaxes. Based on the final fits of the model spectra to the observed ones, we try to interpret the new features in the spectral region between 2.5 and 5.0 μm observed with *AKARI* for the first time.

2. Observations and Data Reduction

The *AKARI*/IRC covered its wavelength range with three independent cameras operated simultaneously, namely the NIR (near-infrared), MIR-S (mid-infrared short), and MIR-L (mid-infrared long) channels. Our observations were all carried out in the AOT (Astronomical Observation Template) IRC04 with parameters of “b;Np” (Lorente et al. 2008). In this mode a grism was used to achieve the highest available spectral resolution; the dispersion was 0.0097 $\mu\text{m}/\text{pixel}$ or

$R = \lambda/\Delta\lambda = 120$ at 3.6 μm (Ohyama et al. 2007). Targets were placed in the $1' \times 1'$ point source aperture mask to minimize the contamination from nearby stars and background sky. The aperture mask was only available for the NIR channel, and the spectra obtained in this programme were limited to the near-infrared wavelength range of 2.5–5.0 μm .

Our target list consisted of 30 brown dwarfs selected by their expected fluxes (to be bright enough for the *AKARI*/IRC instrument to provide high-quality spectra within reasonable number of pointings) and their spectral types (to sample various types from L to T). A pointed observation by *AKARI* allowed about 10 minutes of exposure. At least two observations were requested per target to obtain data redundancy. Due to severe visibility constraint of the satellite, not all requested observations were carried out. There were 18 pointing opportunities for 11 objects in the cryogenic mission phase. A summary of the observed targets is given in Table 1, and the observation record is presented in Table 2. The tables include observations which were not successful, for completeness.

The standard software toolkit *IRCSPEC_RED* (Ohyama et al. 2007) was used for the data reduction¹. The processing was performed in January 2008 with the pre-released version of the toolkit, which should be equivalent with the public version “20080528”. We followed the standard reduction recipe. Fine tuning of the on-source / off-source mask on the spectral images was adopted to obtain the maximum signal and minimum contamination. Corrections of instrumental effects and wavelength / flux calibrations were all done automatically in the toolkit, and we did not observe any calibration sources by ourselves. Since our observations were in principle slitless spectroscopy, the major source of the wavelength error was the determination of the reference point. The typical error was 0.5 pixel of the detector or $\sim 0.005\text{ }\mu\text{m}$ (Ohyama et al. 2007), but could be larger on some occasions. We applied a small correction ($-0.008\text{ }\mu\text{m}$) to 2MASS J152322+3014 by comparing the position of CH₄ Q-branch feature with other objects and with the synthesized spectrum. The overall flux calibration

¹The software is available from the *AKARI* observers’ site; <http://www.ir.isas.jaxa.jp/AKARI/Observation/>

TABLE 1
SUMMARY OF THE TARGETS IN THE CURRENT PROGRAMME

Object Name	R.A.(J2000)	Dec.(J2000)	Sp.Type	[<i>J</i>]	[<i>H</i>]	[<i>K</i>]	[<i>L'</i>]	ref.
2MASS J04151954−0935066	04:15:19.54	−09:35:06.6	T8	15.32	15.70	15.83	13.28	1,3
SDSS J053951.99−005902.0	05:39:52.00	−00:59:01.9	L5	13.85	13.04	12.40	11.32	1,3
2MASS J05591914−1404488	05:59:19.14	−14:04:48.8	T4.5	13.57	13.64	13.73	12.14	1,3
SDSS J083008.12+482847.4	08:30:08.25	+48:28:48.2	L9	15.22	14.40	13.68	11.98	1,3
2MASS J12171110−0311131	12:17:11.10	−03:11:13.1	T7.5	15.56	15.98	15.92	13.96	1,3
GD 165B	14:24:39.09	+09:17:10.4	L3	15.64	14.75	14.09	12.93	1,3
SDSS J144600.60+002452.0	14:46:00.61	+00:24:51.9	L5	15.56	14.59	13.80	12.54 ^a	1,3
2MASS J15232263+3014562	15:23:22.63	+30:14:56.2	L8	15.95	15.05	14.35	12.86	1,5
2MASS J17114573+2232044	17:11:45.73	+22:32:04.4	L6.5	17.09	15.80	14.73	N/A	2
SDSS J175032.96+175903.9	17:50:32.93	+17:59:04.2	T3.5	16.14	15.94	16.02	14.95 ^b	1,4
ϵ Ind Ba+Bb	22:04:10.52	−56:46:57.7	T1+T6	11.91	11.31	11.21	9.97 ^b	2,4

References. — [*J, H, K*] (1) Knapp et al. (2004), (2) 2MASS Point Source Catalog, (3) Golimowski et al. (2004) [*L'*] (4) Patten et al. (2006), (5) Leggett et al. (2002)

^aEstimated magnitude.

^b*Spitzer*/IRAC 3.5 μ m band magnitude.

error is 10 per cent in the middle of the wavelength range and 20 per cent at the short / long edges. See Ohyama et al. (2007) for more details about data reduction and calibration.

3. Near-Infrared Spectra of Brown Dwarfs

Figure 1 shows the observed *AKARI* spectra of brown dwarfs in the sequence of their spectral types from L (bottom) to T (top). When an object was observed twice, the two data sets were processed independently and are plotted in different colors. In general, the two spectra are consistent with each other, demonstrating the high quality and reliability of the data.

The overall SEDs of the observed spectra agree well with the predictions from the previous photometry and theoretical works. The spectra of L-type dwarfs are rather smooth and featureless, mildly peaked at $3.8 \mu\text{m}$ as a result of broad absorption bands of H_2O at shorter wavelengths and CO at longer wavelengths. On the other hand, spectra of T-type dwarfs are dominated by deep molecular absorption features. As expected, we detect CH_4 and H_2O molecular bands. The bands deepen as the spectral type evolves. The band shapes are heavily distorted due to saturation in the latest object, 2MASS J041519–0935 (T8).

The most remarkable finding in the current *AKARI* spectra is a detection of the CO_2 fundamental stretching-mode band at $4.2 \mu\text{m}$ in the late-L and T-type dwarfs. The identification of this band is demonstrated in Figure 2, in which the spectrum of 2MASS J055919–1404 is compared with synthesized spectra of CO_2 . Spectra of CO and PH_3 are also presented for reference. The shape of the band profile, especially a sharp edge around $4.2 \mu\text{m}$ confirms the identification of the feature as CO_2 .

This is the first detection of CO_2 in brown dwarfs, since the wavelength is inaccessible from the ground or even from airborne observations due to huge opacity of the molecule itself in the telluric atmosphere. The band is most apparent in the T4.5 dwarf 2MASS J055919–1404, and is clearly recognized in 2MASS J041519–0935 (T8) and ϵ Ind Ba+Bb (T1+T6). It is seen in the L9 dwarf SDSS J083008+4828 and very marginally in the L8 dwarf 2MASS J152322+3014. We suspect that the formation of the molecule takes place in a rel-

atively low temperature environment.

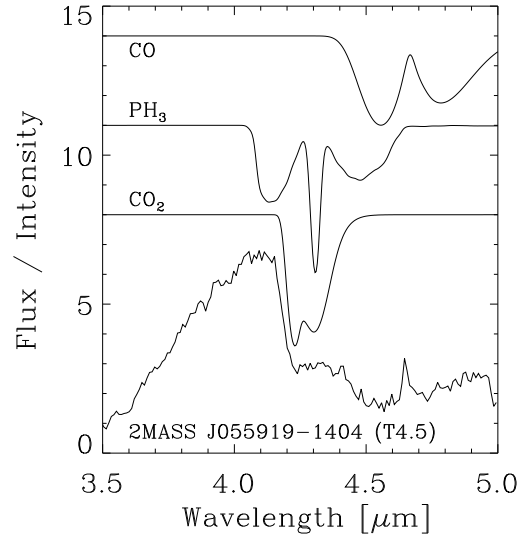


Fig. 2.— The spectrum of 2MASS J055919–1404 is compared with model spectra of CO_2 , PH_3 , and CO. The model spectra are calculated by a simple plane-parallel configuration with column densities and excitation temperatures of; 10^{18} cm^{-2} and 700 K for CO_2 , 10^{19} cm^{-2} and 700 K for PH_3 , and 10^{18} cm^{-2} and 1000 K for CO, respectively. The CO_2 and CO data are taken from HITEMP database (Rothman et al. 1997), and PH_3 data from HITRAN2008 (Rothman et al. 2009). The model spectra are normalized, and scaled and shifted for comparison.

Another important result from our observations is that we see the CO fundamental band in the $4.4\text{--}5.0 \mu\text{m}$ region in all of our samples including the coolest T8 dwarf, 2MASS J041519–0935. The detection of the CO molecule in a late-T dwarf was first reported by Noll, Geballe, & Marley (1997) and Oppenheimer et al. (1998) in the T6 dwarf Gl 229B. Two more objects have been added recently by Geballe et al. (2009); 2MASS J09373487+2931409 (T6) and Gl 570D (T7.5). The presence of the CO band is also suggested from the *Spitzer* $3.5\text{--}7.9 \mu\text{m}$ photometry (Patten et al. 2006; Leggett et al. 2007). Our *AKARI* spectra provide direct and indubitable evidence of the molecule and strongly support the idea that the presence of the CO band is a common feature in the late-T dwarfs.

Table 2: Observation log

Object Name	Date	OBSID	Remarks
2MASS J041519−0935	2007-02-18	1720005-001	Ghosting
2MASS J041519−0935	2007-02-18	1720005-002	Ghosting
2MASS J041519−0935	2007-08-23	5125080-001	Re-observation
2MASS J041519−0935	2007-08-24	5125081-001	Re-observation
SDSS J053951−0059	2006-09-17	1720009-001	
2MASS J055919−1404	2006-09-22	1720006-001	
2MASS J055919−1404	2006-09-22	1720008-001	
SDSS J083008+4828	2006-10-20	1720007-001	
SDSS J083008+4828	2006-10-21	1720007-002	
2MASS J121711−0311	2007-06-26	1720068-001	Too faint
GD165B	2007-07-24	1720074-001	Data lost
SDSS J144600+0024	2007-08-02	1720072-001	
eps Ind Ba+Bb	2006-11-02	1720003-001	
eps Ind Ba+Bb	2006-11-02	1720004-001	
2MASS J152322+3014	2007-01-26	1720002-001	
2MASS J171145+2232	2007-03-05	1720001-001	Too faint
SDSS J175032+1759	2007-03-17	1720050-001	Confusion
SDSS J175032+1759	2007-03-17	1720050-002	Confusion

We also detect the CH₄ molecule in SDSS J053951−0059 (L5), confirming the previous report by Noll et al. (2000) that the molecule is already present in the atmosphere of L5 dwarfs. The feature is not clear in another L5 source SDSS J144600+0024, partly because of its relatively low S/N. The band develops in the L8 dwarf, 2MASS J152322+3014, and starts showing the *P*- and *R*-branches.

Because of moderate spectral resolution it is difficult to identify any more molecules in the spectra.

3.1. Comments on individual objects

3.1.1. SDSS J053951−0059

Fan et al. (2000) selected this object as a high-*z* quasar candidate from the SDSS commissioning image and found it to be an L5 dwarf through follow-up spectroscopy. Due to its relatively high flux level (~ 8 mJy at $3.8 \mu\text{m}$) the quality of the obtained spectrum is good. We can clearly recognize the presence of CH₄ *Q*-branch absorption at $3.3 \mu\text{m}$ on the otherwise rather smooth spectrum.

3.1.2. SDSS J144600+0024

This L5 object was nominated as a brown dwarf by Geballe et al. (2002). Because of relatively low S/N compared to another L5 object SDSS J053951−0059 above, we do not recognize the CH₄ *Q*-branch dip in the spectrum of this source, while the overall SEDs are consistent with each other.

3.1.3. 2MASS J152322+3014

McLean et al. (2000) found that this source is of the latest L-type and assigned it as L8/L9. It was confirmed as L8 by Geballe et al. (2002). This source, together with SDSS J144600+0024, is one of the faintest objects among our current dataset, and the quality of the spectrum is not excellent. However, we clearly see a more developed CH₄ band than in the L5 sources. The CO₂ band is marginally detected.

3.1.4. SDSS J083008+4828

Geballe et al. (2002) classified this object as L8-T0, or L9 as an average. It is on the border of L/T spectral types and is a good example to investigate the transition from L to T. There are rather remarkable changes in the spectral fea-

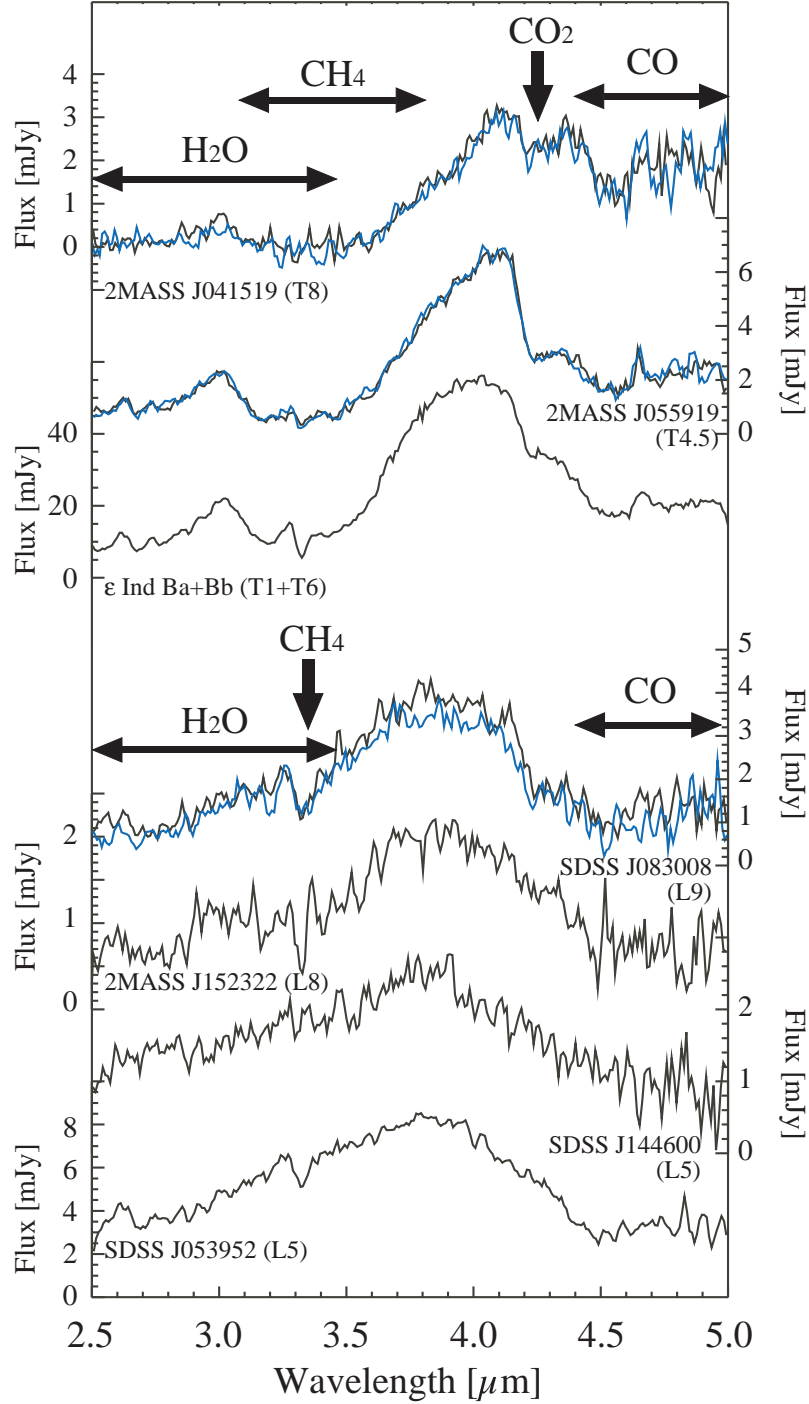


Fig. 1.— The NIR spectra of brown dwarfs obtained by the *AKARI*/IRC. The spectra are ordered in the sequence of their spectral types from bottom (L5) to top (T8). When two observations were made for an object, the data were processed independently and the second spectrum is indicated in blue. The difference between the two observations represents the practical errors. Positions of major molecular bands are indicated.

tures between this source from the previous L8 source 2MASS J152322+3014. We see that H₂O and CO absorption bands become more prominent than earlier L-type sources. The CH₄ *Q*-branch is very clear, but *P*- and *R*-branches are less obvious. The CO₂ band is clearly seen.

3.1.5. ϵ Ind Ba+Bb

This object was identified by Scholz et al. (2003) as a companion to the K5V star, ϵ Ind A. Because of its proximity to the Sun (3.6 pc), it is the brightest among our observed targets. We observed the object twice within a day but found that one observation (OBSID=1720003-1) was significantly degraded by charged particle hits before and during the exposure. The other spectrum (OBSID=1720004-1) shown in Figure 1 clearly exhibits the four major molecular bands; CH₄, H₂O, CO and CO₂. This object is in fact a binary system of T1 and T6 dwarfs, with *K*-band magnitudes of 14 and 16, respectively (McCaughrean et al. 2004). *AKARI*'s spectrum is a mixture of the two spectral types and we will not use it for quantitative analysis.

3.1.6. 2MASS J055919–1404

The object was identified as a ‘warm’ T-dwarf by Burgasser et al. (2000). From a near-infrared spectrum in 0.9–2.3 μ m they concluded that the source was near the L/T transition border. Burgasser et al. (2006b) classified the object as T4.5. The *AKARI* spectra of this dwarf show very deep CO and CO₂ absorptions beyond 4.0 μ m, together with CH₄ and H₂O bands below 3.8 μ m. As a result the spectra show a peak at 4 μ m. A sharp peak, probably the CO band center appears very clearly between the *R*- and *P*-branches. Our observations are consistent with the photometry by Leggett et al. (2002) that the *M'* band flux of this source is fainter by a factor of three than that expected if CO/CH₄ abundance follows thermal equilibrium. Our spectra confirm that CO is the major source of opacity in the wavelength region.

3.1.7. 2MASS J041519–0935

This object was first identified as a T-type brown dwarf by Burgasser et al. (2002) based on near infrared spectroscopy. The object has been designated a “standard” T8 source by

Burgasser et al. (2006b). It is one of the latest spectral-type brown dwarf, and is the coolest object in our sample. The first observations of this target with *AKARI* were carried out in 2007 February. However, the data were considerably contaminated by ghosting from a nearby bright star. We reobserved the object a half year later in 2007 August and obtained a clean spectrum.

The spectra exhibit deep H₂O and CH₄ absorption bands, which are almost completely saturated at the wavelengths below 3.5 μ m. On the other hand, the object has sufficient flux in the longer wavelength range, where we clearly identify the CO and CO₂ bands. Two independent observations show almost identical shape in this wavelength range, strengthening the reality of the detections.

4. Comparisons of the Observed and Model Spectra

In this section, we examine to what extent the newly observed spectra of the 2.5–5.0 μ m region can be explained with the model spectra and what remains unexplained with the present models of the photospheres of cool dwarfs. For this purpose, we apply our Unified Cloudy Model (UCM), a brief description of which is given in Section 4.1. We assume local thermodynamical equilibrium (LTE) throughout this section. Then we outline our method of analysis with some examples in Section 4.2 and the results of our analysis in Section 4.3. The physical parameters estimated by our analysis are summarized in Section 4.4. Finally, we examine the errors and limitation of our analysis based on the UCM in Section 4.5.

4.1. Predicted spectra of dusty dwarfs

Generally, stellar spectra can be interpreted in terms of T_{eff} , $\log g$, chemical composition, and micro-turbulent velocity. However, a new feature in the spectra of brown dwarfs, compared with usual stellar spectra, is the effect of dust clouds formed in the photosphere. If the properties of dust clouds can be defined uniquely from the four basic parameters considered above, the spectra of brown dwarfs could eventually be interpreted in terms of these four parameters, namely T_{eff} , $\log g$, chemical composition, and micro-turbulent velocity. At present, the dependence of the dust

cloud properties on the four basic parameters is unknown, because the formation and disappearance of dust clouds in the photospheres of brown dwarfs is not yet well understood.

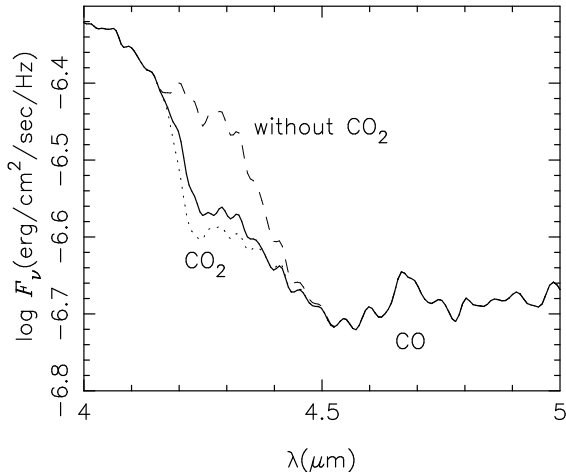


Fig. 3.— The predicted spectrum of a UCM with $T_{\text{eff}} = 1300$ K, $T_{\text{cr}} = 1800$ K, $\log g = 4.5$, $\xi_{\text{micro}} = 1$ km s^{-1} , and Solar metallicity, showing the effect of the CO_2 $4.2 \mu\text{m}$ band based on the line list (solid line) and on the band model opacity (dotted line) compared with the case without CO_2 lines (dashed line).

On the other hand, some observations indicate that the properties of the dust clouds do not necessarily depend uniquely on such basic parameter as T_{eff} . For example, infrared colors such as $J - K$ plotted against T_{eff} show a large variation at a fixed T_{eff} (e.g. Marley et al. 2005; Tsuji 2005). Since these infrared colors depend directly on the properties of the dust clouds, this fact implies that the properties of the dust clouds should be different even for the same T_{eff} . Also, one important observational result is that T_{eff} shows little change over the spectral types between about L5 and T5 (e.g. Golimowski et al. 2004; Nakajima et al. 2004). In other words, the characteristics of the spectra used as signatures of the spectral types are quite different even for the same T_{eff} and hence they are not necessarily determined by T_{eff} . This result implies that the basic features of the spectra of brown dwarfs should be determined by some additional parameter(s) other than T_{eff} . Again dust should play a major role in this respect

as in the case of the infrared colors noted above.

Thus, a major problem is how to consider the effect of dust in the interpretation and analysis of the spectra of brown dwarfs. For this purpose, we apply our Unified Cloudy Model (UCM) in which the dust forms at a layer where temperature is equal to the condensation temperature, T_{cond} , but disappears at somewhat lower temperature which we refer to as the critical temperature, T_{cr} . At this temperature, the radius of the dust grain r_{gr} reaches the critical radius r_{cr} , where the Gibbs energy of condensation is maximum. Then, at this point, dust starts to grow larger and larger, and will precipitate from the gaseous mixture. For this reason, dust disappears in the layers with $T < T_{\text{cr}}$, and will exist only in the layers of $T_{\text{cr}} < T < T_{\text{cond}}$. Thus dust is present in the layers whose photospheric temperatures are within the above range, and this means that a thin dust cloud forms in the photosphere of brown dwarfs, as discussed in more detail elsewhere (Tsuji 2001, 2002). It is to be noted that T_{cond} is defined by the thermodynamical data and is hence fully controlled by T_{eff} and $\log g$ (see e.g. Figure 3 in Tsuji (2002)). On the other hand, T_{cr} is not predictable by any physical theory at present. Instead, T_{cr} is introduced as a free parameter in our UCM, and it serves as a measure of the thickness of the dust cloud (the dust cloud is thicker if the deviation of T_{cr} from T_{cond} is larger).

With the introduction of T_{cr} , the UCM is characterized by the five parameters including T_{cr} in addition to the usual four parameters, T_{eff} , $\log g$, chemical composition, and micro-turbulent velocity. From observations, we showed that at least one additional parameter is needed to describe the observed characteristics of brown dwarfs, and we now propose to identify T_{cr} as the additional parameter required from observations.

A new feature in the *AKARI* observations discussed in Section 3 is the detection of the CO_2 band at $4.2 \mu\text{m}$. Although CO_2 is included in the construction of the UCM as well as in our evaluation of the spectra with the use of the band model opacity (e.g. Appendix of Tsuji 2002), we recompute the spectra with the CO_2 line list from the HITEMP database (Rothman et al. 1997) in view of the detection of the CO_2 band in several objects. As an example, a predicted spectrum including CO_2 based on the line list (solid line) is

compared with that without CO_2 (dashed line) in Figure 3 for a UCM with $T_{\text{eff}} = 1300$ K, $T_{\text{cr}} = 1800$ K, $\log g = 4.5$, $\xi_{\text{micro}} = 1 \text{ km s}^{-1}$, and Solar abundance. For comparison, the result based on the band model opacity is shown by the dotted line. We use the band model opacity during the iterations of model construction but apply the line list in all the computation of the spectra. So far, CO_2 was largely neglected in spectroscopy and model photospheres of cool dwarfs, but the result shown in Figure 3 reveals that the effect of CO_2 absorption is significant even within the framework of the LTE analysis. Since carbon atoms are mostly consumed in CO and/or CH_4 in cool dwarfs, CO_2 cannot be very abundant, but rather large f -values of CO_2 transitions make the molecule an important absorber in the spectra of cool dwarfs.

The major spectral feature in the 2.5–5.0 μm region is the CH_4 fundamental band at 3.3 μm , for which we apply the line list by Freedman (2005, private communication) discussed in detail by Freedman, Marley, & Lodders (2008). Certainly the CH_4 line lists including the high excitation lines are not yet satisfactory as discussed before (Tsuji 2005), but we believe that Freedman’s list is the best one currently available for the fundamental band. Other line lists included are: H_2O (Partridge & Schwenke 1997), CO (Guelachivili et al. 1983; Chackerian & Tipping 1983), OH (Jacquinet-Husson et al. 1999), CN (Cerny et al. 1978; Bauschlicher et al. 1988), and SiO (Lavas, Maki & Olson 1981; Tipping & Chackerian 1981). Also, NH_3 , PH_3 , and H_2S are considered on the basis of the band models. With these spectroscopic data, the spectra between 2.5 and 5.0 μm for our UCMs are evaluated at a resolution of 0.01 cm^{-1} and convolved with the slit function of $\text{FWHM} = 3000 \text{ km s}^{-1}$, which is about the resolving power of the *AKARI* spectrometer. Note that the observed spectra shown in Figures 4, 5, & 6 are smoothed with $R = 100$, and that the error weighted average is taken if two valid spectra are available.

4.2. Method of analysis and some examples

We restrict our analysis to the spectral region between 2.5 and 5.0 μm , which we have observed completely for the first time. Although analyses of different spectral regions do not necessarily pro-

vide the same answer as to what are the best parameters of the photosphere, as shown in detail by Cushing et al. (2008), we restrict our analysis to the 2.5–5.0 μm region for this very reason. In fact, for our purpose stated at the beginning of this Section, it is meaningless to find a solution that provides a good fit to other regions but not to the 2.5–5.0 μm region. We return to this problem in Section 4.5.

We assume that the objects we have observed are all of Solar metallicity (Anders & Grevesse 1989; Allende Prieto et al. 2002) and that the micro-turbulent velocity is near solar (1 km s^{-1}) throughout. Then, major parameters that define the characteristics of a spectrum are T_{eff} , T_{cr} , and $\log g$. In fitting the observed spectrum with the predicted one, we refer to the empirical data summarized in Table 3. We start with the parallaxes by Vrba et al. (2004) which covered our full sample. We notice that their values agree quite well with other results in general. We choose T_{eff} to be T_{eff}^0 close to the so-called empirical T_{eff} suggested by Vrba et al. (2004) (Table 3) and examine the cases of $T_{\text{eff}} = T_{\text{eff}}^0$ and $T_{\text{eff}}^0 \pm 100$ K. As a result, we examine three values of T_{eff} near the empirical T_{eff} . But this choice of trial T_{eff} ’s is not necessarily successful as described below (e.g. a case of 2MASS J055919–1404 to be discussed in Section 4.2). This fact suggests that the so-called empirical T_{eff} cannot be fully realistic as will be discussed in Section 4.4.1. We also consider three cases of $T_{\text{cr}} = 1700, 1800, \& 1900$ K and three values of $\log g = 4.5, 5.0, 5.5$. Thus, we consider $3 \times 3 \times 3 = 27$ combinations of these parameters (T_{eff} , T_{cr} , and $\log g$), and select the case that shows a best fit to the overall shape of the 2.5–5.0 μm SED.

We discuss the procedure outlined above for the case of SDSS J083008+4828 as an example. The empirical T_{eff} of this L9 dwarf is 1327 K (Table 3), but the CH_4 3.3 μm band is too weak for such a low value of T_{eff} . Therefore we start our trials with $T_{\text{eff}} = 1300$ K and extend then to higher T_{eff} , rather than to examine the cases of $T_{\text{eff}} = 1300 \pm 100$ K. It is rather difficult to find a good fit in this object, but one possible solution is obtained for $(T_{\text{eff}}, T_{\text{cr}}, \log g) = (1500, 1700, 4.5)$ from our 27 trial models. The effect of T_{eff} along with the possible best case is shown in Figure 4a: only the case of $T_{\text{eff}}=1500$ K provides a reasonable fit to the

P - and R -branches of CH_4 fundamentals, although the predicted Q -branch is a bit stronger than that in the observed spectrum.

The effect of T_{cr} at fixed values of $T_{\text{eff}} = 1500$ K and $\log g = 4.5$ is illustrated in Figure 4b. Although the fit to the observed CO_2 $4.2 \mu\text{m}$ feature can be improved by higher values of T_{cr} (i.e. with thinner dust cloud), the fit to the CH_4 $3.3 \mu\text{m}$ feature appears to be worse. The effect of $\log g$ is rather modest as shown in Figure 4c, but the lowest gravity of $\log g = 4.5$ provides better fits both to the CH_4 $3.3 \mu\text{m}$ and CO_2 $4.2 \mu\text{m}$ bands than the higher values. The final fit we find, however, is not so good around 2.7 , 4.2 , and $4.5 \mu\text{m}$ and we will discuss these wavelength regions in Section 4.3.

Another example is the case of 2MASS J055919–1404. The empirical T_{eff} of this T4.5 dwarf is 1469 K (Table 3), and we, at first, examined the cases of $T_{\text{eff}} = 1400 \pm 100$ K. It was difficult to find a good fit, but we found that the case of $T_{\text{eff}} = 1300$ provides a relatively close fit to some features. However, an anonymous referee called our attention to a recent result by Cushing et al. (2008) who obtained $T_{\text{eff}} = 1200$ K for this object, and suggested to examine this case. Although this case differs by a large value (≈ 300 K!) from the empirical value, we now include $T_{\text{eff}} = 1200$ K in our trial and find that this case actually provides a better fit as shown in Figure 5a. For example, the relatively strong CH_4 fundamental band can be better explained by $T_{\text{eff}} = 1200$ K than by $T_{\text{eff}} = 1300$ K. However, the CO_2 $4.2 \mu\text{m}$ feature as well as the strong absorption at the positions of CO fundamentals cannot be fitted at all. We will return to this problem in Section 4.3.

If we assume values of T_{cr} lower than 1900 K, the fits to the CH_4 $3.3 \mu\text{m}$ band tend to become worse while those to the CO_2 and possible CO bands show little change as seen in Figure 5b. The $J - K$ color near zero (Table 3) also suggests that the dust cloud is rather thin, consistent with the high value of T_{cr} . The effect of $\log g$ is examined for the fixed values of $T_{\text{eff}} = 1200$ K and $T_{\text{cr}} = 1900$ K. It is found that the spectrum shows little change for the change of $\log g$, but the 2.8 – $3.0 \mu\text{m}$ feature tends to fit better for the lower values of $\log g$ (Figure 5c). We conclude that the case of $(T_{\text{eff}}, T_{\text{cr}}, \log g) = (1200, 1900, 4.5)$ is the best compromise for this object.

4.3. Results

We now extend the same procedure outlined in Section 4.2 to the other objects except for ϵ Ind Ba+Bb because of the composite nature of its spectrum due to its binarity. The observed and predicted spectra can be fitted rather well in the remaining four objects (see Figure 6), and thus they are more or less easier to analyze compared to the cases discussed in Section 4.2. For this reason, we only give the resulting best fits for them². The parameters that give the best fits for all six objects are summarized in Table 4. After we find the possible best model for each object, we measure the vertical shift in logarithmic scale between the observed spectrum and the predicted one based on the best model we found. The emergent flux from the unit surface area of the object, F_ν (in units of $\text{erg cm}^{-2} \text{s}^{-1} \text{Hz}^{-1}$), is written as

$$\log F_\nu = \log f_\nu - 2 \log(R/d) - 23.497,$$

where f_ν (in unit of Jy) is the observed flux, d is the distance to the object based on the measured parallax, and R is the radius of the object. The vertical shift provides R/d . With the known distance, we can estimate the radius R and the result is also given in Table 4. The resulting fits in absolute scale are given in Figure 6.

4.3.1. SDSS J053951–0059

The empirical T_{eff} of this L5 dwarf is 1690 K (Table 3), and we find that the case of $(T_{\text{eff}}, T_{\text{cr}}, \log g) = (1800, 1800, 5.5)$ shows the best fit for this object. In fact, the overall shape of the SED as well as the strengths of the CH_4 Q -branch at $3.3 \mu\text{m}$ and the CO fundamental at $4.6 \mu\text{m}$ is reasonably fit for this case as shown in Figure 6a. It is to be noted that the effect of T_{cr} is of comparable importance to that of T_{eff} . In fact, the column densities of both dust and molecules generally increase at the lower T_{eff} (at fixed T_{cr}) and also at the lower T_{cr} (at fixed T_{eff}). For this reason, the effects of T_{eff} and T_{cr} on the spectra are often difficult to discriminate. We have considered the effects of both T_{eff} and T_{cr} from the beginning, and looked for the best solution. The effect of $\log g$ on

²The numerical details of the predicted spectra and the UCMs are available from <http://www.mtk.ioa.s.u-tokyo.ac.jp/~ttsuji/export/ucmLM,ucm>, respectively.

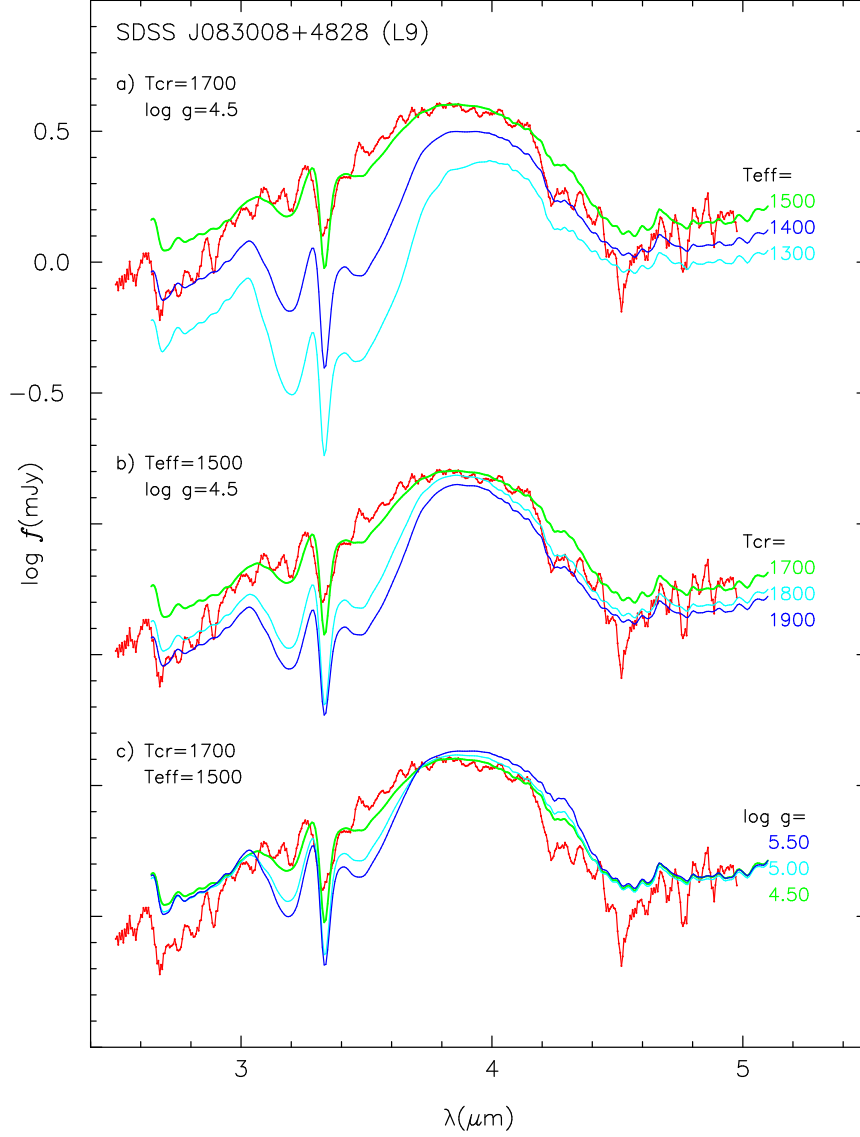


Fig. 4.— The observed spectrum of SDSS J083008+4828 (L9) is compared with the predicted spectra based on the UCM. The best fit obtained for $(T_{\text{eff}}, T_{\text{cr}}, \log g) = (1500, 1700, 4.5)$ is shown in each plot. Flux is adjusted by shifting the model spectra vertically. The same amount of shift is applied to the other predicted spectra. Hence no attempt is made to fit them to the observed spectrum, but are shown here for comparison purposes. a) Effect of T_{eff} under the fixed values of $T_{\text{cr}}=1700$ K and $\log g = 4.5$. b) Effect of T_{cr} under the fixed values of $T_{\text{eff}}=1500$ K and $\log g = 4.5$. c) Effect of $\log g$ under the fixed value of $T_{\text{cr}}=1700$ K and $T_{\text{eff}} = 1500$ K.

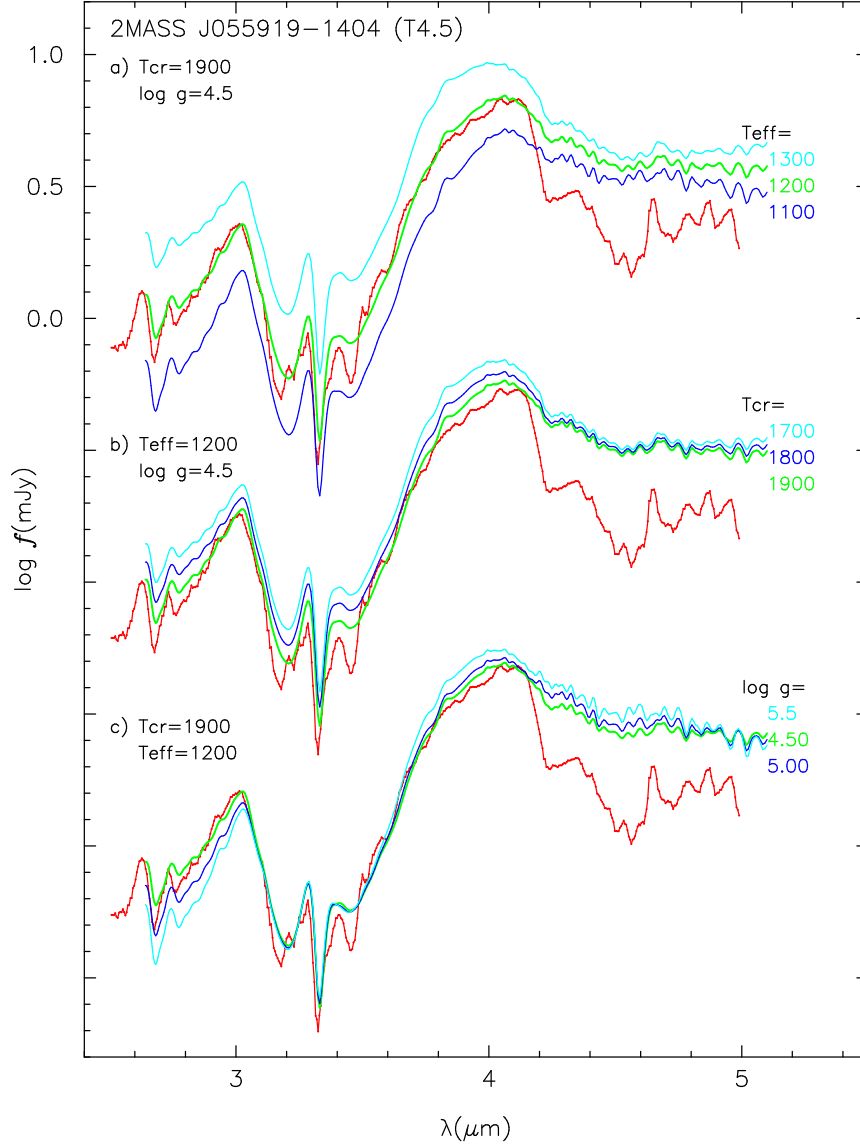


Fig. 5.— The observed spectrum of 2MASS J055919-1404 (T4.5) is compared with predicted spectra based on the UCM. The best fit is obtained for $(T_{\text{eff}}, T_{\text{cr}}, \log g) = (1200, 1900, 4.5)$. See the caption of Figure 4 as for other details. a) Effect of T_{eff} under the fixed values of $T_{\text{cr}}=1900$ K and $\log g = 4.5$. b) Effect of T_{cr} under the fixed values of $T_{\text{eff}}=1200$ K and $\log g = 4.5$. c) Effect of $\log g$ under the fixed value of $T_{\text{cr}}=1900$ K and $T_{\text{eff}} = 1200$ K.

Table 3: The known observed data

no.	object	sp. type ^a Opt./IR	$J - K$ ^b	parallax ^c (marcsec)	T_{eff}^c (K)
1	SDSS J053951-0059	L5/L5	1.45	76.12 ± 2.17	1690 (+173, -137)
2	SDSS J144600+0024	L6/L5	1.76	45.46 ± 3.25	1592 (+175, -140)
3	2MASS J152322+3014	L8/L8	1.60	57.30 ± 3.27	1330 (+142, -112)
4	SDSS J083008+4828	L8/L9	1.54	76.42 ± 3.43	1327 (+140, -111)
5	2MASS J055919-1404	T4.5	-0.16	95.53 ± 1.44	1469 (+153, -122)
6	2MASS J041519-0935	T8	-0.51	174.34 ± 2.76	764 (+88, -71)

Ref.

a) Kirkpatrick (2005) for L and Burgasser et al. (2006b) for T

b) Knapp et al. (2004)

c) Vrba et al. (2004)

Table 4: Basic parameters estimated from the model fittings using UCMs

no.	object	T_{eff} (K)	T_{cr} (K)	$\log g$	R/R_J^a	ΔT_{eff} (K) ^b
1	SDSS J053952-0059	1800	1800	5.5	0.804	-110
2	SDSS J144600+0024	1700	1700	4.5	0.716	-108
3	2MASS J152322+3014	1500	1700	4.5	0.684	-170
4	SDSS J083008+4828	1500	1700	4.5	0.700	-173
5	2MASS J055919-1404	1200	1900	4.5	1.175	-269
6	2MASS J041519-0935	800	T_{cond}	4.5	0.767	-36

a) radius R relative to the Jupiter's radius R_J (see Section 4.3).

b) $\Delta T_{\text{eff}} = T_{\text{eff}}$ (Table 3 by empirical method) - T_{eff} (Table 4 by our model fitting).

the spectrum is rather minor compared with the other parameters, but the lower gravities may be reasonably excluded from the overall poor fits.

The resulting fit in absolute scale (Figure 6a) shows that the spectrum observed by *AKARI* can reasonably be accounted for by our model.

4.3.2. *SDSS J144600+0024*

Although the empirical T_{eff} of this L5 dwarf is near 1600 K (Table 3), we find it very difficult to assume $T_{\text{eff}} < 1600$ K since the observed CH_4 feature at $3.3 \mu\text{m}$ is very weak if present. Again by the procedure outlined in Section 4.2, we find that a case of $(T_{\text{eff}}, T_{\text{cr}}, \log g) = (1700, 1700, 4.5)$ shows the best fit for this object. For example, we see that not only the strength of the CH_4 $3.3 \mu\text{m}$ band but also the overall shape of SED are best fitted with $T_{\text{eff}} = 1700$ K. The effect of T_{cr} is rather large and we can easily exclude such high values of T_{cr} as 1800 and 1900 K. Also, the very red $J-K$ color (Table 3) suggests that the dust cloud is pretty thick and T_{cr} cannot be as high as 1900 K. It is found that the overall SED is again not sensitive to $\log g$, but the strengths of both the CH_4 Q -branch at $3.3 \mu\text{m}$ and CO fundamental band could discriminate the best $\log g$ of 4.5 from the higher values of $\log g = 5.0$ and 5.5.

The resulting fit in absolute scale in Figure 6b shows that the observed spectrum of the $2.5\text{--}5.0 \mu\text{m}$ region, which possesses almost no distinct features, can reasonably be accounted for by our model.

4.3.3. *2MASS J152322+3014*

The empirical T_{eff} of this L8 dwarf is 1330 K (Table 3), but we found that the best fit is found for $(T_{\text{eff}}, T_{\text{cr}}, \log g) = (1500, 1700, 4.5)$. In fact, the modest strength of the CH_4 $3.3 \mu\text{m}$ band suggests that T_{eff} cannot be below 1300 K, and it is only the case of $T_{\text{eff}} = 1500$ K that provides a reasonable fit not only to the Q - but also to the P - and R -branches of the CH_4 fundamental band. We confirm that such a fit as shown for $T_{\text{cr}} = 1700$ K can no longer be found for T_{cr} as high as 1800–1900 K. This result is consistent with the red $J-K$ color of 1.60 (Table 3), which implies that the dust cloud of this L8 dwarf is rather thick. The strength of the CO fundamental band is almost independent of $\log g$, but the P - and R -branches of the CH_4

fundamentals depend on $\log g$ and can only be explained with the low gravity of $\log g = 4.5$. The effect of $\log g$ on the infrared spectrum is again rather modest and accurate determination of $\log g$ is difficult.

A detection of CO_2 at $4.2 \mu\text{m}$ suggested in Section 3 can be well supported by our model prediction that shows a depression at the expected position of the CO_2 $4.2 \mu\text{m}$ band and even shows a reasonable fit quantitatively (see Figure 6c). The fit in the region of the CO fundamental band appears to be poor and the deep absorption features near 4.5 and $4.9 \mu\text{m}$ remain unexplained. We suspect, however, that the CO fundamental band provides the major contribution as in later type dwarfs to be discussed in Section 4.3.4.

Thus the spectrum observed by *AKARI* now shows some dissonances with the predicted spectrum in this late-L dwarf as shown in Figure 6c.

4.3.4. *SDSS J083008+4828*

As already discussed in some detail in Section 4.2, we find $(T_{\text{eff}}, T_{\text{cr}}, \log g) = (1500, 1700, 4.5)$ for this object. The final fit is shown in Figure 6d. We notice that the resulting parameters are the same as that for 2MASS J152322+3014 discussed in Section 4.3.3. This result is also consistent with the similarity of the empirical T_{eff} and of the $J-K$ color between these two late-L dwarfs (see Table 3). Nevertheless, the observed spectra of the two objects differ significantly. For example, the observed feature near the $2.7\text{--}2.9 \mu\text{m}$ region (largely due to H_2O ν_1, ν_3 and $2\nu_2$ bands) shows a large difference between these two objects of the same physical parameters. Since this feature is well reproduced by our models in other objects except for SDSS J083008+4828 (see Figure 6), this should not be due to any systematic effects in our models.

A more interesting result is that the observed CO_2 $4.2 \mu\text{m}$ feature in this object is very strong as noted already (Section 3), and that it is too strong compared with the prediction in marked contrast to the case of 2MASS J152322+3014. It appears that the CO_2 $4.2 \mu\text{m}$ feature cannot be explained by any combination of T_{eff} , T_{cr} , and $\log g$ with our UCM essentially based on the LTE assumption, while those of 2MASS J152322+3014 may be more consistent with the LTE prediction. Such a large

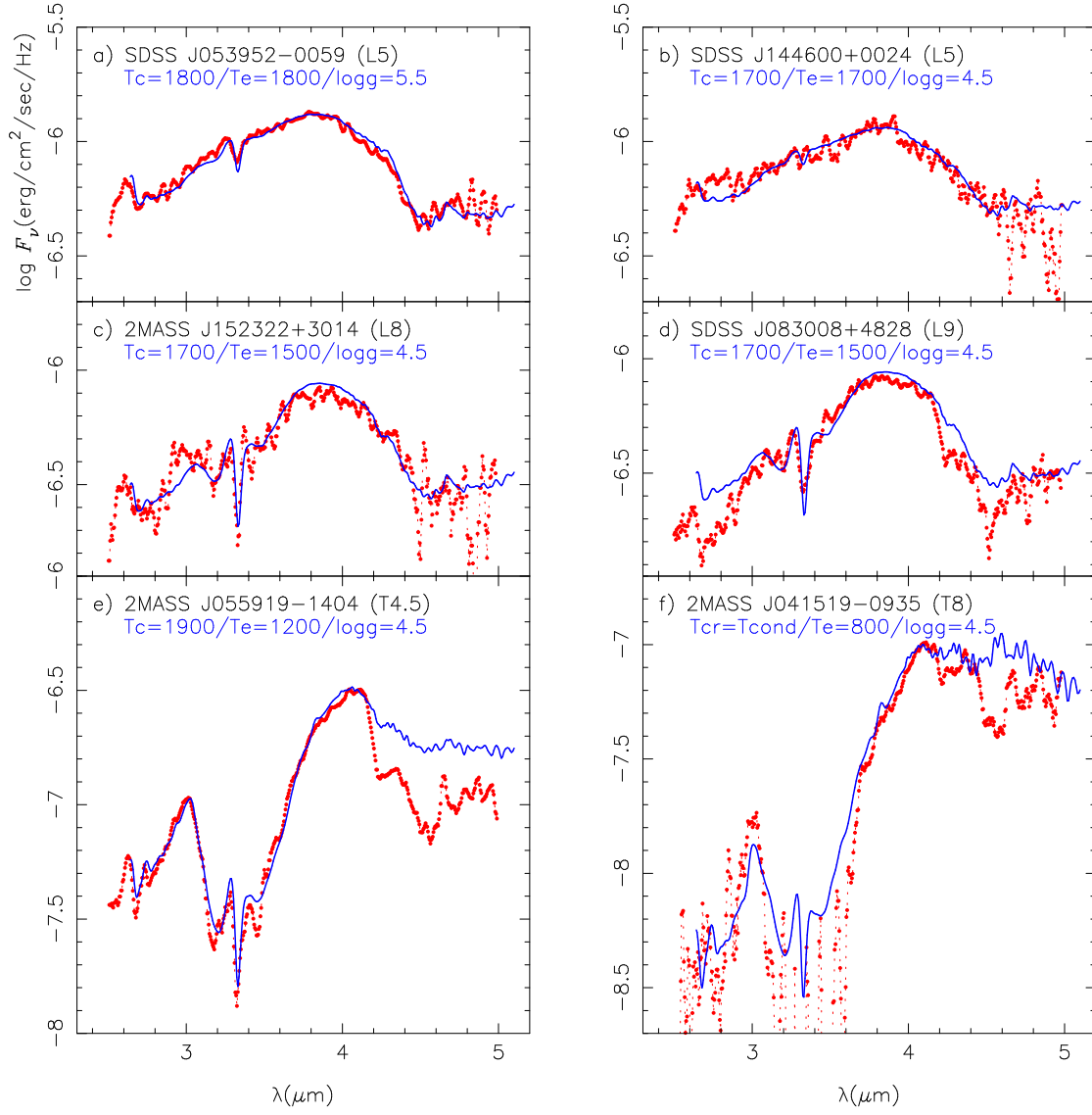


Fig. 6.— The observed and predicted spectra based on the UCMs are compared on an absolute scale: a) SDSS J053951-0059 (L5); b) SDSS J144600+0024 (L5); c) 2MASS J152322+3014 (L8); d) SDSS J083008+4828 (L9); e) 2MASS J055919-1404 (T4.5); and f) 2MASS J041519-0935 (T8).

difference in CO₂ band in the two objects of similar physical parameters cannot be explained by differences in dust cloud properties if, as we find, T_{cr} is nearly the same around 1700 K in both objects. The deep absorption at 4.5 μm can be identified with the *R*-branch of the CO fundamental, but cannot be explained within the framework of the LTE assumption as well.

Thus, there are serious difficulties in understanding the spectrum observed by *AKARI* in that the region between 4 and 5 μm cannot be fitted at all by the LTE prediction based on our UCM.

4.3.5. 2MASS J055919–1404

Details of the model fitting of this object were described in Section 4.2, and our final fit on an absolute scale is shown in Figure 6e. We are shocked to see that the discrepancy between the observed and predicted spectra is so large in the region beyond 4.1 μm . The region of CO *R*-branch is too deep to be explained by our LTE model and CO *P*-branch also appears to be appreciable. Thus we confirm that the CO bands are actually enhanced not only in late-T dwarfs but also in mid-T dwarfs, as anticipated by photometric observations (e.g. Leggett et al. 2007).

In this object, a more important result is that the new spectrum observed by *AKARI* provides definite evidence for the presence of the strong CO₂ band in brown dwarfs for the first time. The depression at 4.2 μm is too large to be accounted for by the predicted CO₂ band and the discrepancy between the observed and predicted spectra is quite serious. All these new features due to CO and CO₂ cannot be accounted for by the present LTE model such as our UCM. In contrast to these serious disagreements in the region beyond 4 μm , the observed and predicted spectra agree quite well in the region between 2.5 and 4.1 μm .

Recent analysis of the SED of this object by Cushing et al. (2008) concluded that $T_{\text{eff}} = 1200$ K, $\log g = 5.5$ and $f_{\text{sed}} = 4$, where f_{sed} is the cloud sedimentation efficiency parameter and a larger value implies greater sedimentation efficiency resulting in a thinner cloud (Ackerman & Marley 2001). Thus f_{sed} is a parameter that may have a similar role as our T_{cr} , with larger f_{sed} corresponding to higher T_{cr} . Thus

their result showing relatively large value of $f_{\text{sed}} = 4$ is consistent with our relatively high value of $T_{\text{cr}} = 1900$ K, and we agree with them on the properties of the dust cloud in this T4.5 dwarf. We also agree that $T_{\text{eff}} = 1200$ K for this object. Thus our results for the cloud properties as well as for T_{eff} show good agreements with those by Cushing et al. (2008), despite the fact that different spectral regions are analyzed with different models. Unfortunately, the results for gravity differ considerably. However, SEDs are not very sensitive to the gravity and this is the parameter most difficult to determine from the model fittings (as will further be discussed in Section 4.4.2).

In summary, some dissonances between the observed and predicted spectra, seen in the late-L dwarfs, appear to be quite distinct in this mid-T dwarf.

4.3.6. 2MASS J041519–0935

The empirical T_{eff} of this T8 dwarf is 764 K (Table 3) and, if a dust cloud forms, it is situated below the layer of the optical depth unity in such a very cool dwarf. For this reason, the spectrum no longer depends on T_{cr} , as we have actually confirmed. Accordingly, we apply the dust-free models in which dust grains have all precipitated just after they are formed (this means $T_{\text{cr}} = T_{\text{cond}}$), and we find the best possible fit for $(T_{\text{eff}}, T_{\text{cr}}, \log g) = (800, T_{\text{cond}}, 4.5)$.

Determination of the physical properties of the coolest brown dwarfs including 2MASS J041519–0935 has been discussed by Burgasser, Burrows & Kirkpatrick (2006a), who calibrated the strengths of H₂O bands and relative fluxes in terms of T_{eff} and $\log g$. As a result, they suggested $T_{\text{eff}} = 740$ –760 K and $\log g = 4.9$ –5.0 for this object. Also, Saumon et al. (2007) suggested a similar result of $T_{\text{eff}} = 725$ –775 K and $\log g = 5.00$ –5.37 based on the analysis of a spectrum including new data obtained with *Spitzer Space Telescope*. Our result is reasonably consistent with these results, although the values of $\log g$ differ from each other. Thus analyses of the different spectral regions by the different models show more or less consistent results in this object at least for T_{eff} .

The overall fit of the predicted spectrum of the possible best model is not so bad (see Figure 6f), but we confirm that the region of the

CO bands cannot be fitted at all. Such a possible large discrepancy in the predicted and observed CO bands in late-T dwarfs was previously suggested based on the ground based observation of Gl 229B (Noll, Geballe, & Marley 1997; Oppenheimer et al. 1998), and more recently for two other late-T dwarfs by Geballe et al. (2009). We confirm these previous results and add a new case of largely enhanced CO fundamentals in late-T dwarfs. We also note that the R -branch is much stronger compared with the P -branch.

A more interesting result is that the CO_2 band at $4.2\ \mu\text{m}$ appears quite distinctly in this late-T dwarf too. It is impossible to explain both the CO and also the CO_2 bands by the LTE models, and we will discuss such cases in the Section 5.

In conclusion, the new spectral region explored by *AKARI* for the first time reveals: first, the enhancement of the CO fundamental bands is a general feature and, second, the CO_2 band at $4.2\ \mu\text{m}$ appear to be an important absorber, in late-L and T dwarfs.

4.4. Basic physical parameters of six brown dwarfs

We now discuss briefly the resulting T_{eff} , T_{cr} , $\log g$, and R/R_J values summarized in Table 4. Also, we discuss briefly the effects of other basic parameters, namely chemical composition (in Section 4.4.4) and micro-turbulent velocity (in Section 4.4.5), which we assumed to be the Solar. If we try to determine these two parameters by the same way as we have done in Section 4.2 and 4.3 for the three basic parameters, we must consider at least $3 \times 3 \times 3 \times 3 = 243$ models instead of 27 models for each object, but this is clearly impractical. Moreover, we do not think that the chemical abundances and micro-turbulent velocity can be determined from such low resolution spectra as those we have at hand.

4.4.1. Effective temperature and radius

We notice first that our T_{eff} 's do not agree with the so-called empirical effective temperatures obtained from the observed luminosities and a constant radius such as $R = 0.9 R_J$ (Vrba et al. 2004) (see 7-th column of Table 4). In fact, we already notice through Section 4.3.1 and 4.3.6 that the observed SEDs cannot be fitted well with

the predicted ones assuming the empirical T_{eff} by Vrba et al. (2004). The reliability of the empirical T_{eff} largely depends on the accuracy of the values of the radius. The constant radius of $R = 0.9 R_J$ was based on a statistical analysis by Burgasser (2001) of the evolutionary models of cool dwarfs by Burrows et al. (1997), but it is unknown if it is appropriate to apply such a value to all the objects.

It is known that the radii of cool substellar objects are independent of mass to within 30 per cent for a broad range of masses from 0.3 to $70 M_J$ (Burrows et al. 2001). The resulting radii of all our six objects (Table 4) appear to be consistent with the prediction of the evolutionary models and confirm that the radii of ultracool dwarfs are within approximately 30 per cent of Jupiter's radius. The mean radius for our six objects is $0.81 R_J$, and thus we agree with Burgasser (2001) in that the radii of ultracool dwarfs are statistically smaller than Jupiter's radius. However, the variation of radii among brown dwarfs appears to be appreciable (Table 4) and may not be represented by a single mean value. For this reason, the so-called empirical effective temperature cannot be completely reliable. Although we use it as a guideline in our analysis (Sections 4.2 & 4.3), it may even be misleading as we showed in the case of 2MASS J055919–1404 (Section 4.2).

Also, because of such variations of the radii in real ultracool dwarfs, an attempt to analyze the observed spectra on an absolute scale based on an assumed radius of $R = R_J$ (Tsuji 2005) does not necessarily work well. For example, we showed before that the near infrared spectrum of 2MASS J152322+3014 observed with Subaru, reduced to an absolute scale with the known parallax and with the assumption of $R = R_J$, agreed with the predicted spectrum of $T_{\text{eff}} = 1300\text{ K}$. For this reason, we suggested T_{eff} of this object to be $\approx 1300\text{ K}$ (Tsuji 2005). However, we find that the shape of the *AKARI* spectrum can be best explained by $T_{\text{eff}} = 1500\text{ K}$ (Section 4.3.3), and that a consistency with the SED on an absolute scale can be achieved if we abandon the ad hoc assumption of $R = R_J$ (see Figure 6c).

In conclusion, we believe that the observed spectrum (or relative SED) can provide a more direct and realistic estimation of the effective temperature of an individual object. Further, an em-

pirical estimation of the radius can be possible if the SED can be reduced to an absolute scale with the known parallax. With this conclusion, we now think it inappropriate to analyze the observed spectrum in absolute scale based on an ad hoc assumption of $R = R_J$, as we proposed before (Tsuji 2005).

4.4.2. Gravity

The determination of $\log g$ is more difficult since the low-resolution infrared spectra depend little on $\log g$, as can be seen in our Figures 4 & 5. Also, this difficulty is clearly shown by a goodness-of-fit (statistic G_k defined by Equation (1) in Cushing et al. (2008) and shown in their Figure 5, in which G_k only shows minor changes for different $\log g$'s (possibly except for no cloud case).

Inspection of Table 4 reveals that our result appears to be biased towards low gravity, namely $\log g = 4.5$ for 5 out of 6 objects. This may be due to the difficulty of gravity determination noted above, at least partly, or may be simply because our sample mostly consists of low gravity objects by chance. We examine if this may be due to any systematic effects in our UCMs. Our gravity determination is essentially based on the gravity dependence of the gas and dust opacities, but we are using more or less standard methods in treating molecular and dust opacities. Also, a comparative study of different modeling approaches did not reveal any systematic effect in our models (Helling et al. 2008). Thus we cannot identify any systematic effect in our models. We hope to examine this problem further with a larger sample in future.

Cushing et al. (2008) used ultracool dwarf evolution models to transfer their (T_{eff}, R) values to (T_{eff}, g) values, from which they obtained $\log g = 4.7$ for 2MASS J055919–1404. This result differs from their result based on their spectral fitting referred to in Section 4.2 ($\log g = 5.5$), but agrees rather well with our value given in Table 4 ($\log g = 4.5$). Thus this result can be supporting evidence for our $\log g$, despite some difficulties noted above. However, the results based on the evolutionary sequences may suffer more or less similar difficulty to the spectral fitting method, since it depends critically on the physical parameters such as T_{eff} , which cannot be very accurate if they are based on the spectral fitting in the limited

spectral region (as will be detailed in Section 4.5).

Given the radius and $\log g$, it is in principle possible to estimate the mass. However, SEDs are not so sensitive to $\log g$ and its accuracy is rather low. For this reason, we believe it impossible to obtain a reasonable mass estimates from our spectra.

4.4.3. Critical temperature

Inspection of Table 4 reveals that the resulting T_{cr} 's show a variety of values in our limited sample, and this result implies that the dust cloud properties differ significantly among different objects. In modeling dusty dwarfs, it is still difficult to determine the dust cloud properties from the basic physics, and we had to introduce such an empirical parameter as T_{cr} to represent the dust cloud properties, at least partly. Other models of dusty dwarfs also have a more or less similar feature. For example, Ackerman & Marley (2001) introduced the cloud sedimentation efficiency f_{sed} in their models and, as discussed in Section 4.3.5, their f_{sed} and our T_{cr} consistently showed that the dust cloud in 2MASS J055919–1404 is rather thin. We hope that a larger sample will be analyzed to clarify the nature of dust clouds and that the result will serve as a guide towards a more physical theory of cloud formation in dusty dwarfs.

4.4.4. Chemical composition

We assumed that the chemical composition in such unevolved objects as brown dwarfs should be the same as the Solar composition. However, the Solar composition itself is by no means well established yet. For example, we adopted $\log A_{\text{C}} = 8.60$ and $\log A_{\text{O}} = 8.92$ (on the scale of $\log A_{\text{H}} = 12.0$) in our initial version of UCM based on the latest results known at that time (Tsuji 2002). However, these values were revised to be $\log A_{\text{C}} = 8.39$ and $\log A_{\text{O}} = 8.69$ based on the three-dimensional(3D) time-dependent hydrodynamical model of the solar photosphere (Allende Prieto et al. 2002) and our present version of UCM is based on these revised values as noted previously (Tsuji et al. 2004). These values are close to the more recent values of $\log A_{\text{C}} = 8.43$ and $\log A_{\text{O}} = 8.69$ (Asplund et al. 2009). Since a direct determination of abundances in brown dwarfs cannot be expected in the near future, we think it best for now to use the most reliable Solar composition.

Unlike the cases of evolved stars in which the surface chemical composition may suffer drastic variations due to convective dredge-up of the products of nuclear processing in the interior, large variations of the surface chemical composition may not be expected in brown dwarfs, but a possibility of small variations may not be excluded. As an example, we examine the effect of carbon abundance on CO and CO₂ features in J083008+4828 and J055919–1404, since CO and CO₂ features in these objects could not be reproduced well with the composition we have assumed. For this purpose, we compute two spectra with log A_C changed by ± 0.15 dex compared to the standard composition we have assumed, namely, log $A_C = 8.39$.

The results for J083008+4828 are shown in the upper diagram of Figure 7. The effect of increasing log A_C by 0.15 dex results in a considerable strengthening of the methane bands, but the overall fitting tends to be worse (compare c with a in the figure). The CO₂ and CO bands at 4.2 and 4.6 μm , respectively, however, do not show any strengthening. The effect of decreasing log A_C by 0.15 dex is rather modest (see d in the figure). The results for J055919–1404 are shown in the lower diagram of Figure 7. The effect of changing log A_C by ± 0.15 dex can be noticed on the CH₄ bands, but CO₂ and CO bands remain almost unchanged. We conclude that the large discrepancies between the observed and predicted CO and CO₂ bands in J083008+4828 and J055919–1404 cannot be the problem of the carbon abundance.

4.4.5. Micro-turbulent velocity

We have assumed the micro-turbulent velocity to be the Solar value of 1 km s^{−1} throughout. Just to see the effect of the micro-turbulent velocity, we increase it to be 2 km s^{−1} and the resulting spectra are compared with those for the case of 1 km s^{−1} for J083008+4828 and J055919–1404 in the upper and lower diagrams, respectively, of Figure 7. Clearly, dependence on the micro-turbulent velocity is quite small (compare a and b in Figure 7) as expected for such high density photospheres dominated by the pressure broadening.

4.5. Errors and limitations of the present analysis based on the UCMs

Since we examine the effect of T_{eff} by steps of 100 K, our T_{eff} cannot be more accurate than ± 50 K. Further, combined with the similar uncertainty in T_{cr} , the final uncertainty in our estimation of T_{eff} may be ± 100 K. But we should notice that the parameters we have found are simply those that explain the *AKARI* spectra in the 2.5–5.0 μm region. We tried more or less similar analysis of the 1.0–2.5 μm region of our objects and found some differences in the resulting parameters, although the differences are mostly within the errors outlined above. In other words, the solution obtained by fitting other spectral regions may not in general explain the 2.5–5.0 μm spectra. As summarized in Figure 6, we are trying to reach a unified understanding of the series of new spectra observed for the first time by *AKARI* covering from mid-L to late-T dwarfs. For this purpose, we believe it best to apply the parameters obtained from the *AKARI* spectra themselves and analyze all our sample consistently.

As shown by Cushing et al. (2008), the effective temperatures obtained by fitting a limited spectral region differ from those obtained by fitting the full SED (0.95–14.5 μm) by typically ≈ 200 K and by as large as 700 K in the worst case. As noted above, we confirm essentially the same difficulty with our UCM. The reason for this difficulty may be because the present models are far from perfect. For example, we do not know the exact form of the dust opacities which suffer from many unknown effects (e.g. composition, size, shape, impurity etc.) and of the molecular opacities based on imperfect line lists. Moreover, we do not know yet the exact nature of the dust clouds formed in the photosphere of cool dwarfs. For these reasons, we think it difficult to expect such rigorous numerical accuracy for brown dwarfs as realized in model photospheres of ordinary stars. We intended from the beginning that our models can at least be of some help as a guide in interpretation and analysis of the observed data of ultracool dwarfs (e.g. Tsuji 2001).

A more perfect model would allow us to more safely analyze a wider spectral region. However, current models of brown dwarf atmospheres are far from perfection. Fitting of a wider spectral region

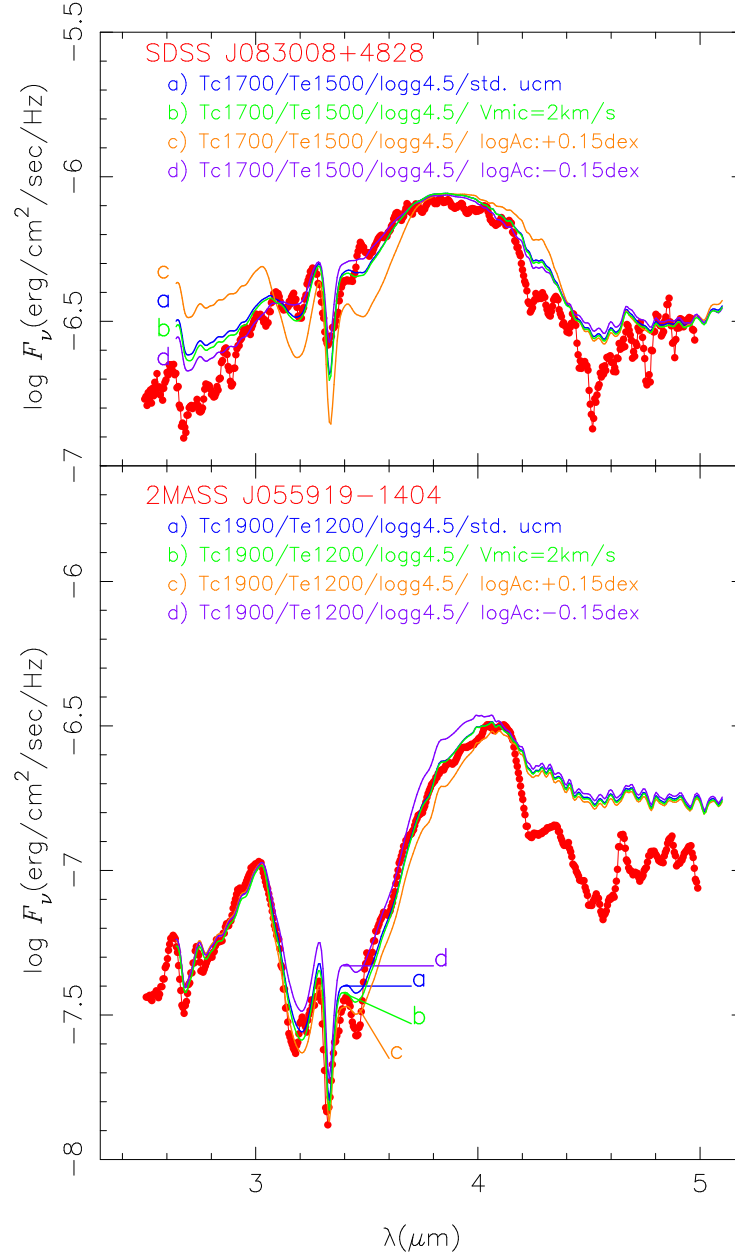


Fig. 7.— The effects of changing $\log A_C$ by ± 0.15 dex and of increasing the micro-turbulent velocity from 1 to 2 km s^{-1} are shown for J083008+4828 in the upper diagram. The same effects are shown for J055919-1404 in the lower diagram.

may sample more regions of uncertain opacities at the same time, and is by no means easier to have better results. Thus we must allow for additional uncertainties beyond those found by fitting one spectral region. We fully agree with Cushing et al. (2008) who concluded that the accurate determination of the physical parameters is still an elusive goal, even though SED fitting method shows reasonable success in general.

For now, we must be satisfied in that our SED fitting analysis based on our UCM has also been done fairly consistently for the new spectral region observed by *AKARI*. The UCM is a semi-empirical model in which the property of the dust clouds is represented by a single parameter T_{cr} and, for this very reason, our UCM is free from yet unknown details of the cloud formation processes. Thus, our UCM can be flexible enough to interpret the major characteristics of the observed spectra in terms of a few basic physical parameters. The UCM, however, assumes LTE throughout and hence cannot be applied directly to the observed features showing possible deviations from LTE. We will discuss such a case in the next section.

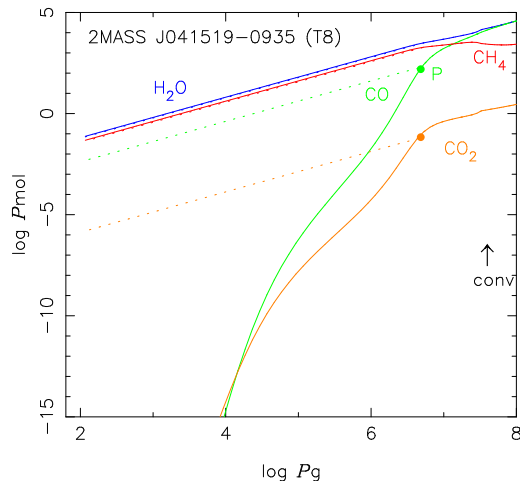


Fig. 8.— Molecular abundances, presented as partial pressure vs total pressure (pressure in units of dyn cm^{-2}), in LTE (solid lines) and in non-equilibrium modified by vertical mixing for the case of $b = 0.1$ (dashed lines) in the photosphere of the T8 dwarf 2MASS J041519-0935 (Model: $T_{\text{eff}}/T_{\text{cr}}/\log g = 800 \text{ K}/T_{\text{cond}}/4.5$). The arrow indicates the onset of convection.

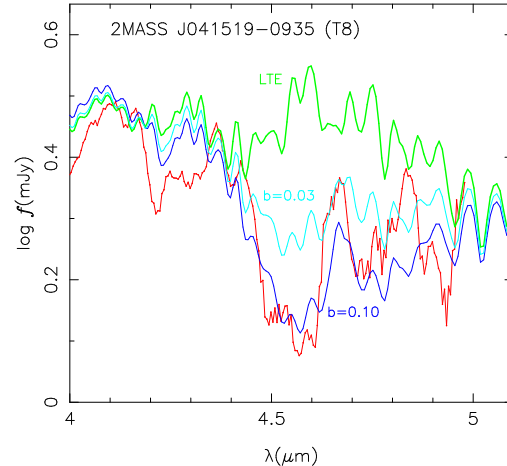


Fig. 9.— The effect of vertical mixing on the CO spectrum in 2MASS J041519-0935 (T8): The cases of LTE, $b = 0.03$, and $b = 0.10$ are compared with the observed spectrum.

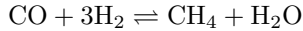
5. Spectral features unexplained by the LTE models

In the previous section, the overall SEDs can be understood reasonably well with the UCM based on LTE, but the observed features of CO and CO_2 in T-dwarfs (and possibly late-L dwarfs) cannot be fitted at all with the spectra predicted by the model. As for CO, this fact has been known for late-T dwarfs (e.g. Noll, Geballe, & Marley 1997; Oppenheimer et al. 1998; Geballe et al. 2009), and we confirm this fact by the better quality data for T8 dwarf 2MASS J041519-0935 (Figure 6f). But we also find that CO bands are enhanced significantly already in the mid-T dwarf 2MASS J055919-1404 (Figure 6e) as well as in the late-L dwarf SDSS J083008+4828 (Figure 6d). A new and more difficult problem is that the CO_2 band at $4.2 \mu\text{m}$ is enhanced enormously in all the cool dwarfs later than L9.

5.1. Late-T dwarf

The unexpected detection of CO in the late-T dwarf Gl 229B has been interpreted as due to vertical mixing of CO from the warm layers where CO is still abundant to the cooler layers where CO is mostly transformed to CH_4 under LTE. This is possible since CO is so stable that the time scale

τ_{chem} of the reaction



is very slow compared to the mixing time scale τ_{mix} (Griffith & Yelle 1999; Saumon et al. 2000), and a detailed computation including such a non-equilibrium effect has been carried out (e.g. Saumon et al. 2007; Hubeny & Burrows 2007).

We try to explain our observations by a simple computation as follows: We show the LTE molecular abundances of CO, H₂O, CH₄, and CO₂ in the photosphere of 2MASS J041519–0935, using the UCM of $(T_{\text{eff}}, T_{\text{cr}}, \log g) = (800 \text{ K}, T_{\text{cond}}, 4.5)$, by the solid lines in Figure 8. We assume that the time scale of CO destruction τ_{chem} is equal to the timescale of mixing τ_{mix} at a depth point P in Figure 8 and CO/CH₄ abundance ratio is fixed at the value b of that point. We examine several values of b . The case of $b = 0.10$ is shown in Figure 8 as an example. The resulting non-equilibrium abundance of CO is indicated by the dashed line. If H₂O and CO₂ abundances relative to CO are fixed at the values at P as are CH₄, H₂O as well as CH₄ abundances in the upper layers should be decreased and the results are also shown by the dashed lines. The decreases, however, are rather minor and difficult to see in the figure. On the other hand, CO₂ abundance shows a large increase as seen by the dashed line in Figure 8.

We compute the spectra based on the non-equilibrium abundances for $b = 0.03$ and $b = 0.1$ together with that of the full LTE, and the results are compared with the observed spectrum of 2MASS J041519–0935 in Figure 9. Inspection of the figure reveals that the observed CO spectrum of 2MASS J041519–0935 can roughly be accounted for with $b = 0.1$. However, the predicted CO₂ band is still too weak compared with the observation even for $b = 0.1$. Of course, there is no reason why CO₂/CH₄ ratio can be fixed at the value at point P, since chemical reaction time-scale of CO₂ cannot be the same as for CO. Further, there is little possibility that more CO₂ can be dredged-up, since CO₂ abundance in the deeper layers is not as large as shown in Figure 8.

On the other hand, it is possible that CO₂ abundance will change to the equilibrium value of the local physical condition if the chemical time scale related to CO₂ formation is not as slow as

in the case of CO. However, if CO₂ attains its equilibrium value with the abundant CO resulting from vertical mixing, CO₂ abundance will be too large. In fact, CO₂ is more abundant than CO at $\log P_g < 4.0$ in LTE as can be inferred from the solid lines in Figure 8. For this reason, we cannot assume simply that CO₂ can be in equilibrium with CO. We cannot predict the precise value of CO₂ abundance without more detailed non-equilibrium analysis, but we can expect from the above consideration that the CO₂ abundance can be somewhat larger than those shown by the dashed line in Figure 8 in the surface layers of 2MASS J041519–0935 and hence the CO₂ band could then be stronger than those suggested in Figure 9.

5.2. Mid-T dwarf

A new result of the *AKARI* observation is that the mid-T dwarf 2MASS J055919–1404 also shows much stronger CO and CO₂ bands than those predicted with the use of the UCM based on LTE. We show the LTE molecular abundances in the photosphere of 2MASS J055919–1404, using the UCM of $(T_{\text{eff}}, T_{\text{cr}}, \log g) = (1200 \text{ K}, 1900 \text{ K}, 4.5)$, by the solid lines in Figure 10.

We first try the vertical mixing model used for the late-T dwarf 2MASS J041519–0935. We again assume that the time scale of CO destruction τ_{chem} is equal to the timescale of mixing τ_{mix} at a point P in Figure 10 and the CO/CH₄ abundance ratio is fixed to a value b at this point. We again test a few values of b . A case of $b = 0.50$ is shown in Figure 10. The resulting non-equilibrium abundance of CO is indicated by the dashed line. Also, H₂O and CO₂ abundances relative to CO are fixed at the values at P and shown by the dashed lines in Figure 10.

We compute the spectra based on the non-equilibrium abundances for $b = 0.1$ and $b = 0.5$ together with those based on the LTE values, and the results are compared with the observed spectrum of 2MASS J055919–1404 in Figure 11. The predicted spectra for non-equilibrium CO and CO₂ abundances show additional depression in the region of CO $R+P$ -branches but little change in the $4.2 \mu\text{m}$ region, compared to the predicted one for the LTE case. This result indicates that the observed CO band can be explained at least partly by the vertical mixing model, but the observed

CO₂ remains completely unexplained. The observed CO feature is still too deep compared with the predicted one, but this may be due to the effect of the deep CO₂ feature whose origin is still unknown.

We conclude that the very strong CO band observed in 2MASS J055919–1404 by *AKARI* can be at least partly explained by the vertical mixing model but the CO₂ feature cannot at all.

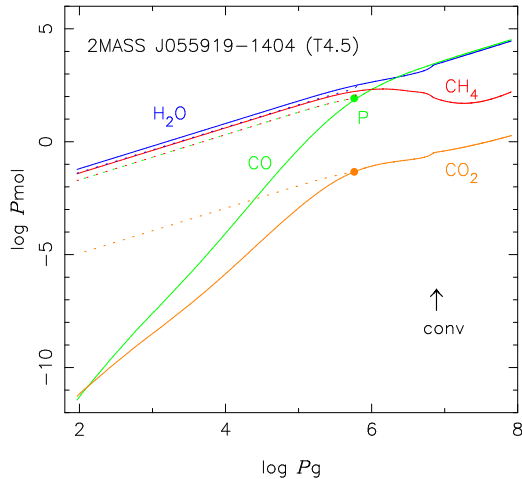


Fig. 10.— Molecular abundances in LTE (solid lines) and in non-equilibrium by vertical mixing for the case of $b = 0.5$ (dashed lines) in the photosphere of T4.5 dwarf 2MASS J055919–1404 (Model: $(T_{\text{eff}}, T_{\text{cr}}, \log g) = (1200 \text{ K}, 1900 \text{ K}, 4.5)$). The arrow indicates the onset of convection.

5.3. Late-L dwarf

We detected a deep absorption around $4.5 \mu\text{m}$ in the late-L dwarf SDSS J083008+4828 and it can be identified with the CO *R*-branch. The *R*-branch tends to be deeper than *P*-branch in CO because of narrower line separation. We notice such a structure of the CO fundamental consisting of the deep *R*-branch and weak *P*-branch in 2MASS J055919–1404, and this similarity lends support in identifying the $4.5 \mu\text{m}$ feature in SDSS J083008+4828 as due to the *R*-branch of CO in the relatively low-quality spectrum of this source (see also, Figure 1), even though the presence of such a deep CO feature is quite unexpected in L-dwarfs. We also see that the $4.2 \mu\text{m}$ feature is very strong.

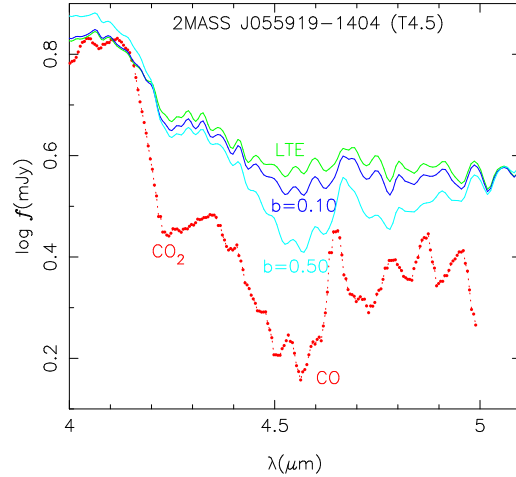


Fig. 11.— Predicted spectra in LTE and in non-equilibrium by vertical mixing ($b = 0.10$ and 0.50) compared with the observed one of T4.5 dwarf 2MASS J055919–1404.

In SDSS J083008+4828, the observed CO band is quite strong while CH₄ band is fairly weak. These observed features imply that CO is quite abundant, and we confirm this possibility in Figure 12 where LTE abundances of CO, CO₂, CH₄, and H₂O are shown based on the UCM of $(T_{\text{eff}}, T_{\text{cr}}, \log g) = (1500 \text{ K}, 1700 \text{ K}, 4.5)$. Inspection of Figure 12 reveals that the CO abundance under LTE is already at its maximum possible value (i.e. almost all the carbon is in CO). Then, vertical mixing, if present, cannot supply additional CO to the upper photosphere and has little effect on the CO band strengths. Thus, without any computation of the spectrum, it is clear that the vertical mixing model cannot be applied to this late-L dwarf. Given that an increase of the CO abundance in the photosphere can no longer be possible (Figure 12), not only by vertical mixing but also by any other method, some changes in the structures of the photosphere and/or in the atmosphere are required to produce the unusually deep CO band observed.

The large strengthening of the CO₂ band cannot be due to vertical mixing either, since CO₂ abundance relative to other molecules is smaller in the deeper layers (Figure 12) and hence vertical mixing will reduce rather than enhance the CO₂ abundance in the upper layers. This result sug-

gests that a non-equilibrium process other than vertical mixing is needed to explain the large enhancement of the CO₂ band.

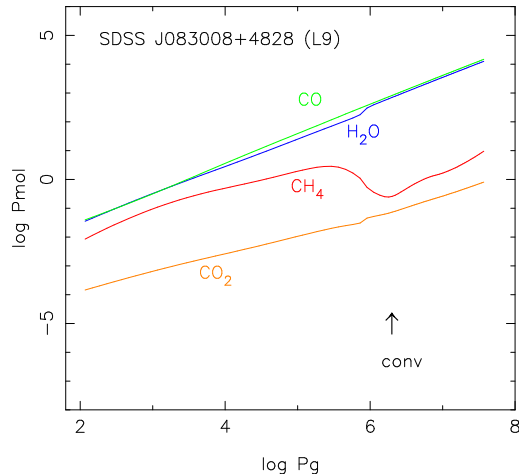


Fig. 12.— Molecular abundances in LTE (solid lines) in the photosphere of the L9 dwarf SDSS J083008+4828 (Model: $(T_{\text{eff}}, T_{\text{cr}}, \log g) = (1500 \text{ K}, 1700 \text{ K}, 4.5)$). A sudden change of H₂O and CO₂ abundances at $\log P_g \approx 6.0$ is due to formation of silicate (MgSiO₃). The arrow indicates the onset of convection.

5.4. Vertical mixing and/or other possibilities

Our analysis confirms that the vertical mixing model can be applied to T-dwarfs at least for CO. This result certainly shows that the vertical mixing model provides one possible way to explain the CO anomaly, but this fact may not necessarily imply that it is a unique solution for this phenomenon. However, our analysis cannot prove the applicability of the vertical mixing model to the late-L dwarfs.

One problem is that the convective zone is actually situated rather deep in the photosphere of cool dwarfs (e.g. Tsuji 2002), although it is said that cool dwarfs are fully convective. For example, the upper boundary of the convective zone is indicated by the arrow in Figures 8 & 10, and the layers where vertical mixing is expected are well above the convective zone. Hence vertical mixing cannot be due to convective mixing. Then, the problem is the unknown mechanism of efficient

mixing in the photosphere of T-dwarfs.

A more difficult problem is how to understand the enhancement of CO₂ bands at 4.2 μm in late-L and T dwarfs throughout. We confirm that this phenomenon cannot be explained by the vertical mixing model at all. So the question is whether the enhancements of CO and CO₂ bands in late-L and T dwarfs are due to the same mechanism. It is still possible that an unknown process resulting in the enhancement of CO₂ will also result in the CO anomaly. In any case, the vertical mixing model cannot have general applicability, and we must look for a more unified model that can be applied to CO and CO₂ in L and T-dwarfs. Presently, we have no solution yet as to the reason why CO₂ (and also CO at least partly) are so strong in these objects. If non-equilibrium processes play major roles, we wonder why the departure from LTE can be so significant in the brown dwarf photosphere, where local density is so high that LTE condition can be naturally satisfied.

More recently, Stephens et al. (2009) analyzed the 0.8–14.5 μm region spectra of many L–T dwarfs and determined not only effective temperature, surface gravity and grain sedimentation efficiency but also vertical gas transport efficiency, based on the models of Saumon & Marley (2008). They showed that vertical mixing improves the fits and the observed spectra were fitted well in general. It will be interesting to check whether their models can explain the enhanced CO bands in late-L dwarfs.

6. Discussion and Concluding Remarks

AKARI provides the first and unique opportunity to take brown dwarf spectra in the important wavelength range 2.5–5.0 μm continuously without interference of telluric atmosphere. In particular, molecular bands of CO, CH₄, and CO₂ altogether in one spectrum present a great advantage for investigating chemical processes in the atmospheres of ultracool dwarfs, through quantitative analysis of their carbon budgets. *AKARI* reveals many remarkable features of ultracool dwarfs. Our observations confirm the presence of CO molecules in the brown dwarf atmospheres of all spectral types from L to very late T-type objects. The fact that all observations ever made for the late-T dwarfs detected CO molecules implies that the

non-equilibrium chemical composition is a common property of the late-T dwarfs.

It has been discussed that this non-equilibrium abundance is due to vertical mixing in the upper photosphere. The CO fundamental band in the T8 dwarf 2MASS J041519–0935 and the T4.5 dwarf 2MASS J055191–1404 can be accounted for by the vertical mixing model (Section 5.1). The idea is also supported by Saumon et al. (2006), and by Mainzer et al. (2007) based on the analysis of the mid-infrared spectrum of T7.5 dwarf Gl 570D taken by *Spitzer*/IRS. They found that the abundance of the NH₃ molecule in the object is almost one order of magnitude smaller than that expected under equilibrium conditions. It is considered that fresh N₂ molecules are continuously provided from inside. Also, the vertical mixing model is shown to be consistent with the photometry of a larger sample of brown dwarfs obtained with *Spitzer*/IRAC (Patten et al. 2006; Leggett et al. 2007).

However, our observations reveal that the CO fundamental band is stronger than predicted by the LTE models in the late-L dwarf (SDSS J083008+4828). Since, unlike in T-dwarfs, CO is already highly abundant in the upper photosphere of these objects, no appreciable increase of CO abundance and hence of the CO band strength can be expected by additional CO from the deeper warm layers. For this reason, some mechanism(s) other than vertical mixing should be looked for in late-L dwarfs. This quest is further strengthened by the detection of CO₂ by *AKARI* as discussed below.

A new piece of information provided by *AKARI* is the detection of CO₂ molecule. The CO₂ band is never observable from the ground, and its 4.2 μ m band is just outside of *Spitzer*/IRS coverage. Gas phase CO₂ in stellar atmospheres was first detected in late-type giants by *ISO*/SWS observations. It was rather unexpected that in addition to the stretching-mode absorption band at 4.2 μ m, the bending mode ro-vibrational bands in the 15 μ m region are often seen in these stars, sometimes in emission (Ryde et al. 1998; Justtanont et al. 1998). The CO₂ band is generally stronger than those expected from the LTE models, implying that some kinds of non-equilibrium processes, either formation of the molecule or radiative excitation, might play a role in the atmospheres of such stars. The sit-

uation is of course quite different in brown dwarfs, with lower temperature and much higher surface density than in red giants. Some amount of the CO₂ molecule is expected under LTE conditions in brown dwarf atmospheres. Though the relative abundance with respect to that of H₂O and CH₄ is small (Figures 8, 10, & 12), the high f -value of this molecule helps to form a rather strong absorption band at 4.2 μ m region as shown in Section 4.1 (see Figure 2). However, a simple comparison with the model tells us that observed absorption is much stronger than expected.

We estimate the temperatures and column densities of the extra CO₂ and CO absorption components in 2MASS J055919–1404 and SDSS J083008+4828. The observed spectra are divided by the best fit UCM spectra shown in Figure 6, and the residual spectra are fitted by two-layers plane-parallel model with given excitation temperature T_{ex} and column density N for each molecule. In this simple model we adopt a Gaussian line width of FWHM = 30 km s^{−1} based upon measurements of H₂O lines by high-resolution spectroscopy in the J-band (McLean et al. 2007). Because of the simplicity of the model, the fitting results are suitable mainly for order of magnitude discussions. The excitation temperature is only mildly constrained by the band shape. Nevertheless, we obtain $(T_{\text{ex}}, N)_{\text{CO}_2} = (800 \text{ K}, 5 \times 10^{17} \text{ cm}^{-2})$ and $(T_{\text{ex}}, N)_{\text{CO}} = (1000 \text{ K}, 2 \times 10^{20} \text{ cm}^{-2})$ for 2MASS J055919–1404, and $(T_{\text{ex}}, N)_{\text{CO}_2} = (800 \text{ K}, 2.5 \times 10^{17} \text{ cm}^{-2})$ and $(T_{\text{ex}}, N)_{\text{CO}} = (1000 \text{ K}, 1.5 \times 10^{19} \text{ cm}^{-2})$ for SDSS J083008+4828, respectively. The results for 2MASS J055919–1404 are presented in Figure 13 as an example. Considering that CO molecules with higher excitation temperature may be located in a slightly interior portion of the photosphere, the ratio of the column densities $N_{\text{CO}_2}/N_{\text{CO}} = 2 \times 10^{-2} \sim 3 \times 10^{-3}$ indicates lower limits of the abundance ratio of the two molecules. It is found that CO₂ is obviously overabundant compared to CO than predicted by the UCM (Figures 10 & 12). This implies that non-equilibrium processes other than vertical mixing may play a role in determining the molecular abundances especially for CO₂.

Another possibility is the presence of extended atmosphere beyond the hydrostatic photospheres, similarly in the case of red-giants. It is interest-

ing that *Spitzer*/IRS observation did not detect any clear CO₂ bands in the 15 μ m region in any brown dwarfs (Roellig et al. 2004; Cushing et al. 2006; Saumon et al. 2006; Mainzer et al. 2007). If the CO₂ molecular layer is extended, emission beyond the photosphere could compensate for the absorption and the observed band strength would be weakened. This effect is usually more effective at longer wavelengths. Of course, there is a more conventional explanation that the heavy opacity of H₂O veils the wavelength region completely. The H₂O opacity reaches a minimum around 4 μ m and makes the 4.2 μ m band visible. If this is the case, the CO₂ molecules would be located in the same layer, or in layers internal to the H₂O. This may be a constraint on constructing chemical models of the brown dwarf atmospheres. High dispersion spectroscopy in the 4 & 15 μ m region from space is an ideal tool for investigating this problem.

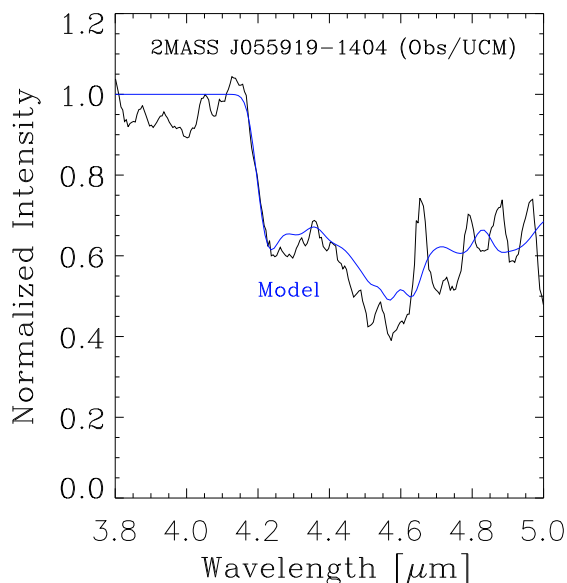


Fig. 13.— The *AKARI* spectrum of 2MASS J055919-1404 is divided by the best fit UCM model and shown in black. Blue line indicates the fitted model spectrum by a plane-parallel configuration with the excitation temperature and the column density of $(T_{\text{ex}}, N)_{\text{CO}_2} = (800 \text{ K}, 5 \times 10^{17} \text{ cm}^{-2})$ and $(T_{\text{ex}}, N)_{\text{CO}} = (1000 \text{ K}, 2 \times 10^{20} \text{ cm}^{-2})$, respectively.

Although non-equilibrium conditions for the

CO/CH₄ and NH₃/N₂ ratios appeared to be explained by the vertical mixing model at least in late-T dwarfs, the unexpected detection of CO₂ by *AKARI* casts doubt as to whether the vertical mixing model alone could explain the carbon chemistry even in late-T dwarfs. In fact, there is no reason why we expect excess CO₂ by the vertical mixing model (Section 5.2) and there should be some other mechanism to produce excess CO₂. A yet unknown mechanism may affect not only CO₂, but also CO as well. In fact, such a new mechanism could also be what we need to explain the enhancement of CO in late-L to mid-T dwarfs for which the vertical mixing model failed.

We continue the *AKARI* brown dwarf programme with the near-infrared channel of the IRC in the “post-Helium” phase (Phase 3). More targets are being observed to cover the spectral ranges from M, L, to T. With the enhanced data set we hope to better understand the some of the current mysteries of ultracool dwarfs.

We thank an anonymous referee for critical reading of the manuscript and constructive comments especially that helped to revise the analysis of Section 4.2. We are grateful to Dr. Gandhi Poshak for his careful checking of the manuscript and many suggestions to improve the text. Dr. Tadashi Nakajima is appreciated for helpful discussions at an initial phase in making this observing programme. Satoko Sorahana gave us useful comments. This research is based on observations with *AKARI*, a JAXA project with the participation of ESA. Issei Yamamura acknowledges JSPS/KAKENHI(C) No.22540260. Takashi Tsuji thanks to the support by JSPS/KAKENHI(C) No.17540213. This research has made use of the SIMBAD database, operated at CDS, Strasbourg, France.

Facilities: *AKARI* (IRC).

REFERENCES

- Ackerman, A. S., & Marley, M. 2001, *ApJ*, 55, 872
- Allende Prieto, C., Lambert, D. L., & Asplund, M. 2002, *ApJ*, 573, L137
- Anders, E., & Grevesse, N. 1989, *Geochim. Cosmochim. Acta*, 53, 197

- Asplund, M., Grevesse, N., Sauval, J., & Scott, P. 2009, *ARA&A*, 47, 481
- Bauschlicher, C. W., Langhoff, S. R., & Taylor, P. R. 1988, *ApJ*, 332, 531
- Becklin, E. E. & Zuckerman, B. 1988, *Nature*, 336, 656
- Burgasser, A. J. 2001, PhD thesis “The Discovery and Characterization of Methane Bearing Brown Dwarfs and the Definition of the T Spectral Class”, California Institute of Technology
- Burgasser, A. J., Burrows, A., & Kirkpatrick, J. D. 2006, *ApJ*, 639, 1095
- Burgasser, A. J., et al. 1999, *ApJ*, 522, L65
- Burgasser, A. J., et al. 2000, *AJ*, 120, 1100
- Burgasser, A. J., et al. 2002, *ApJ*, 564, 421
- Burgasser, A. J., Geballe, T. R., Leggett, S. K., Kirkpatrick, J. D., Golimowski, D. A. 2006, *ApJ*, 637, 1067
- Burrows, A., Hubbard, W. B., Lunine, J. I., Liebert, J. 2001, *Rev. Mod. Phys.*, 73, 719
- Burrows, A., et al. 1997, *ApJ*, 491, 856
- Cerny, D., Bacis, R., Guelachvili, G., & Roux, F. 1978, *J. Mol. Spectros.*, 73, 154
- Chackerian, C. Jr. & Tipping, R. H. 1983, *J. Mol. Spectrosc.*, 99, 431
- Cushing, M. C., et al. 2006, *ApJ*, 648, 614
- Cushing, M. C., et al. 2008, *ApJ*, 678, 1372
- Fan, X., et al. 2000, *AJ*, 119, 928
- Freedman, R. S., Marley, M., & Lodders, K. 2008, *ApJS*, 174, 504
- Geballe, T. R., et al., 2002, *ApJ*, 564, 466
- Geballe, T. R., et al. 2009, *ApJ*, 695, 844
- Golimowski, D. A., et al. 2004, *AJ*, 127, 3516
- Griffith, C. A., & Yelle, R. V. 1999, *ApJ*, 519, L85
- Guelachivili, G., De Villeneuve, D., Farrenq, R., Urban, W., & Verges, J. 1983, *J. Mol. Spectros.*, 98, 64
- Helling, Ch., et al. 2008, *MNRAS*, 391, 1854
- Hubeny, I., & Burrows. A. 2007, *ApJ*, 669, 1248
- Jacquinet-Husson, N., et al. 1999, *J. Quant. Spec. Radiat. Transf.*, 62, 205
- Justtanont, K., Feuchtgruer, H., de Jong, T., Cami, J., Waters, L.B.F.M., & Yamamura, I. 1998, *A&A*, 330, L17
- Kawada, M., et al. 2007, *PASJ*, 59, S389
- Kirkpatrick, J. D. 2005, *ARA&A*, 43, 195
- Kirkpatrick, J. D., Henry, T. J., Liebert, J. 1993, *ApJ*, 406, 701
- Kirkpatrick, J. D., et al. 2000, *AJ*, 120, 447
- Knapp, G. R. et al. 2004, *AJ*, 127, 3553
- Lavas, F. J., Maki, A. G., & Olson, W. B. 1981, *J. Mol. Spectros.*, 87, 449
- Leggett, S. K., Saumon, D., Marley, M. S., Geballe, T. R., & Fan, X. 2007, *ApJ*, 655, 1079
- Leggett, S. K., et al. 2002, *ApJ*, 564, 452
- Lorente, R., et al., 2008, “AKARI IRC Data User Manual Version 1.4”, <http://www.ir.isas.jaxa.jp/AKARI/Observation/>
- MacCaughrean, M. J., Close, L. M., Scholz, R.-D., Lenzen, R., Biller, B., Brandner W., Hartung, M., & Lodieu, N. 2004, *A&A*, 413, 1029
- McLean, I. S., Prato, L., MacGovern, M. R., Burgasser, A. J., Kirkpatrick, J. D., Rice, E. L., Kim, S. S. 2007, *ApJ*, 658, 1217
- McLean, I. S., et al. 2000, *ApJ*, 533, L45
- Mainzer, A. K., et al. 2007, *ApJ*, 662, 1245
- Marley, M., Cushing, M. C., & Saumon, D. 2005, *ESA SP-560*, 791
- Murakami, H., et al. 2007, *PASJ*, 59, S369
- Nakajima, T., Tsuji, T., & Yanagisawa, K. 2004, *ApJ*, 607, 499
- Nakajima, T., et al. 1995, *Nature*, 378, 464
- Noll, K. S., Geballe, T. R., Leggett, S. K., & Marley, M. S., 2000, *ApJ*, 541, L75

- Noll, K. S., Geballe, T. R., & Marley, M. S., 1997, *ApJ*, 489, L87
- Ohyama, Y., et al. 2007, *PASJ*, 59, S411
- Onaka, T., et al. 2007, *PASJ*, 59, S401
- Oppenheimer, B. R., Kulkarni, S. R., Matthews, K., & Nakajima, T. 1995, *Science*, 270, 1478
- Oppenheimer, B. R., Kulkarni, S. R., Matthews, K., & van Kerkwijk, M. H., 1998, *ApJ*, 502, 932
- Partridge, H., & Schwenke, D. W. 1997, *J. Chem. Phys.*, 106, 4618
- Patten, B.M., et al. 2006, *ApJ*, 651, 502
- Roellig, T. L., et al., 2004, *ApJS*, 154, 418
- Rothman, L. S. 1997, “High-temperature molecular spectroscopic database”, (CD-ROM) (Andover: ONTAR Co.)
- Rothman, L. S., et al., 2009, *J. Quant. Spec. Radiat. Transf.*, 110, 533
- Russell, H. N. 1934, *ApJ*, 79, 317
- Ryde, N., Eriksson, K., Gustafsson, B., Lindqvist, M., Olofsson, H. 1998, *Ap&SS*, 255, 301
- Saumon, D., & Marley, M. S. 2008, *ApJ*, 689, 1327
- Saumon, D., Marley, M. S., Cushing, M. C., Leggett, S. K., Roellig, T. L., Lodders, K., & Freedman, R. S., 2006, *ApJ*, 647, 552
- Saumon, D., et al. 2000, *ApJ*, 541, 373
- Saumon, D., et al. 2007, *ApJ*, 656, 1136
- Scholz, R.-D., McCaughrean, M. J., Lodieu, N., & Kuhlbrod, B., 2003, *A&A*, 398, L29
- Stephens, D. C., et al. 2009, *ApJ*, 702, 154
- Tipping, R. H., & Chackerian, C., Jr. 1981, *J. Mol. Spectros.*, 88, 352
- Tsuji, T. 1964, *Ann. Tokyo Astron. Obs.*, 2nd Ser., 9, 1
- Tsuji, T. 2001, in *Ultracool Dwarfs – New Spectral Types L and T*, ed. H. R. Jones & I. A. Steele (Berlin: Springer-Verlag), 9
- Tsuji, T. 2002, *ApJ*, 575, 264
- Tsuji, T. 2005, *ApJ*, 621, 1033
- Tsuji, T., Nakajima, T., & Yanagisawa, K. 2004, *ApJ*, 607, 511
- Tsuji, T., Ohnaka, K., Aoki, W., & Nakajima, T. 1996, *A&A*, 308, L29
- Vrba, F. J. et al., 2004, *AJ*, 127, 2948